

**1 Convective response to changes in the**  
**2 thermodynamic environment in idealized weak**  
**3 temperature gradient simulations**

Sharon L. Sessions,<sup>1</sup> Michael J. Herman,<sup>1</sup> and Stipo Sentić<sup>1</sup>

---

Corresponding author: S. L. Sessions, Department of Physics and Geophysical Research Center,  
New Mexico Tech, Socorro, NM 87801, USA. (sessions@kestrel.nmt.edu)

<sup>1</sup>Department of Physics and Geophysical  
Research Center, New Mexico Tech,  
Socorro, NM, USA.

4 **Abstract.** We investigate the response of convection to idealized pertur-  
5 bations in the thermodynamic environment in simulations which parame-  
6 terize the large scale circulations using the weak temperature gradient (WTG)  
7 approximation. The perturbations include a combination of modifying the  
8 environmental moisture and atmospheric stability via imposing anomalies  
9 in reference moisture and temperature profiles. We find that changes in at-  
10 mospheric stability strongly influence the character of convection by dras-  
11 tically modifying the vertical motion profile, whereas changes to atmospheric  
12 moisture modulate the intensity of precipitation produced by the convection,  
13 but do not qualitatively change the shape of the vertical motion profile.

14 An important question is how does horizontal moisture advection into the  
15 domain affect convection? We test several different parameterizations of this  
16 process; these include lateral entrainment by circulations induced by enforc-  
17 ing WTG, a moisture relaxation which parameterizes the advection of mois-  
18 ture by large scale non-divergent circulations, and control simulations in which  
19 both of these mechanisms are turned off so horizontal advection is assumed  
20 negligible compared to vertical advection. Interestingly, the most significant  
21 differences resulting from the choice of horizontal moisture advection scheme  
22 appear in environmental conditions which suppress—rather than support—the  
23 development of deep tropical convection. In this case, lateral entrainment re-  
24 lated to WTG circulations is the only parameterization which results in ex-  
25 treme drying of the troposphere in environments which suppress convection.

<sup>26</sup> Consequently, this is the only parameterization which permits multiple equilibria–  
<sup>27</sup> dry or precipitating steady states–in convection.

## 1. Introduction

28 Understanding the interaction between deep tropical convection and the large scale en-  
29 vironment benefits our knowledge of the tropical atmosphere and leads to improvements  
30 in the convective parameterizations in forecast and climate models. This interaction is  
31 two-way: convection fuels waves that drive the large scale transport, while the large scale  
32 circulation sets the environment for convection. In this work, we focus on the latter part  
33 of this interaction and investigate how the characteristics of convection respond to changes  
34 in the large scale thermodynamic environment, where the large scale environment is pa-  
35 rameterized using the weak temperature gradient approximation [*Sobel and Bretherton,*  
36 *2000; Raymond and Zeng, 2005*].

37 The weak temperature gradient (WTG) approximation is based on the observation  
38 that horizontal temperature gradients are small in the tropical atmosphere where gravity  
39 waves act to balance convective heating and radiative cooling. Models employing the  
40 WTG approximation achieve this balance by generating a domain-mean vertical velocity  
41 that counteracts buoyancy anomalies produced by diabatic processes. This WTG vertical  
42 velocity—and thus the modeled convection—is sensitive to changes in the reference profiles  
43 of potential temperature and moisture which represent the thermodynamic environment  
44 [*Mapes, 2004; Raymond and Sessions, 2007; Wang and Sobel, 2012; Emanuel et al., 2013;*  
45 *Wang et al., 2013; Herman and Raymond, 2014*]. It is also sensitive to the model and the  
46 specific implementation of WTG [*Daleu et al., 2012; Herman and Raymond, 2014*], as well  
47 as to details of how horizontal moisture advection is parameterized [*Sobel and Bretherton,*  
48 *2000; Sobel et al., 2007*].

49 The purpose of this investigation is twofold: 1) to diagnose the changes in convection  
50 modeled in different thermodynamic environments using the WTG approximation, and  
51 2) to determine how different choices for parameterizing horizontal moisture advection  
52 affects the convection. We also consider how these influence the existence of multiple  
53 equilibria in precipitation.

54 Several modeling studies have demonstrated the sensitivity of convection to the thermo-  
55 dynamic environment—characterized here by atmospheric stability and humidity. *Mapes*  
56 [2004] used a cloud resolving model to investigate the transient rainfall response to deep  
57 vertical and vertical-dipole perturbations in potential temperature and water vapor mix-  
58 ing ratio. While both of these perturbations—representing first and second baroclinic  
59 mode vertical displacements, respectively—generated transient responses in rainfall, *Mapes*  
60 [2004] found that the vertical-dipole perturbations enhanced the transient rainfall response  
61 compared to deep vertical displacements. *Raymond and Sessions* [2007] and *Herman and*  
62 *Raymond* [2014] showed that more stable environments produce more bottom-heavy con-  
63 vection with increased precipitation rates, while more moist environments produce more  
64 intense convection without changing the altitude of the maximum mass flux. An inter-  
65 esting contrast is found in results of *Wang and Sobel* [2012], who showed that strong  
66 lower tropospheric drying can reduce top-heaviness and ultimately prevent deep convec-  
67 tion entirely, though this did not occur in a similar investigation when convection was  
68 also parameterized [*Sobel and Bellon*, 2009].

69 The sensitivity of convection to the thermodynamic environment is not unique to WTG  
70 simulations; alternate parameterizations of the large scale also produce responses broadly  
71 consistent with WTG simulations. For example, *Kuang* [2010] computed linear response

72 functions based on the response of convection to temperature and moisture perturbations.  
73 His results were corroborated in a parallel study by *Tulich and Mapes* [2010], who con-  
74 sidered transient sensitivities of convection to sudden perturbations in temperature and  
75 moisture.

76 Idealized studies which investigate how convection responds to prescribed changes in  
77 the thermodynamic environment—and how the response depends on the implementation  
78 of WTG—provide valuable insight for identifying mechanisms involved in convective pro-  
79 cesses. These studies also provide a framework for interpreting WTG simulations which  
80 incorporate observed anomalies in reference profiles of WTG simulations, such as those  
81 used to study the MJO [*Wang et al.*, 2013].

82 Previous studies have demonstrated the importance of vertical moisture advection on  
83 the existence of convectively coupled waves [e.g., *Kuang*, 2008]. Another important aspect  
84 of this work is to determine how the sensitivities of convection to the thermodynamic  
85 environment depend on the method used to parameterize horizontal moisture advection.  
86 This is potentially important for improving the representation of convection in global  
87 models [*Derbyshire et al.*, 2004], as well as for improving the simulation of the Madden-  
88 Julian Oscillation [*Pritchard and Bretherton*, 2014; *Zhu and Hendon*, 2015].

89 Another important application of WTG simulations is investigating whether a particu-  
90 lar set of parameters support multiple equilibria in precipitation. Multiple equilibria refers  
91 to the ability of a model to either sustain a dry or precipitating steady state under identi-  
92 cal boundary conditions; the state realized by the model depends on the initial moisture  
93 profile in the model [*Sobel et al.*, 2007; *Sessions et al.*, 2010; *Emanuel et al.*, 2013; *Herman*  
94 *and Raymond*, 2014]. Previous studies indicate that the existence of multiple equilibria

95 depends on the degree to which WTG is enforced [Sessions et al., 2010], domain size  
96 [Sessions et al., 2010], boundary layer depth [Herman and Raymond, 2014], how environ-  
97 mental moisture is chosen to enter the domain [Sobel et al., 2007], and the background sea  
98 surface temperature in which the multiple equilibria experiments are performed [Emanuel  
99 et al., 2013], among other things.

100 Whether or not the thermodynamic environment or choice for horizontal moisture ad-  
101 vection scheme affects the existence of multiple equilibria is important for understanding  
102 the relevance of these choices in large scale representations. For example, multiple equi-  
103 libria in WTG domains is believed to be analogous to convecting and dry regions of  
104 large domain radiative convective equilibrium simulations with self-aggregated convection  
105 [Bretherton et al., 2005; Muller and Held, 2012; Wing and Emanuel, 2013; Emanuel et al.,  
106 2013; Jeevanjee and Romps, 2013]. Wing and Emanuel [2013] and Emanuel et al. [2013]  
107 demonstrated the importance of the feedback between radiative cooling and water va-  
108 por in self-aggregation and multiple equilibria experiments, respectively; thus, identifying  
109 parameters which influence water vapor content in these WTG experiments may help  
110 identify mechanisms relevant for organizing convection.

111 This paper is organized as follows: We briefly introduce the weak temperature gradient  
112 approximation and its implementation in our model in section 2. In section 3, we describe  
113 the model and the series of numerical experiments used for this work. Diagnostic quantities  
114 are defined in section 4, we present results in section 5, and we summarize and discuss  
115 the consequences of our results in section 6.

## 2. Weak temperature gradient (WTG) approximation

116 The weak temperature gradient (WTG) approximation is a useful tool for investigating  
 117 convection in limited domain simulations [*Sobel and Bretherton, 2000; Raymond and Zeng,*  
 118 *2005*]. This work uses an implementation of WTG similar to that used by *Raymond and*  
 119 *Zeng* [2005], but with some significant upgrades which primarily result in changes to  
 120 the source terms in the equations governing the equivalent potential temperature,  $\theta_e$ ,  
 121 and the total water mixing ratio,  $r_t$ . For the purpose of this work, the most important  
 122 changes are: different representations for parameterizing horizontal moisture advection  
 123 from the environment into the model domain (“moisture treatment”); and performance  
 124 improvements and bug fixes (described in the model documentation, not here). These  
 125 changes are documented in *Herman and Raymond* [2014]; though we summarize those  
 126 pertinent to this work here.

The thermodynamic equations for equivalent potential temperature,  $\theta_e$ , and total water mixing ratio,  $r_t$ , are:

$$\frac{\partial \rho \theta_e}{\partial t} + \nabla \cdot (\rho \mathbf{v} \theta_e - K \nabla \theta_e) = \rho (S_{es} + S_{er} - S_e) \quad (1)$$

and

$$\frac{\partial \rho r_t}{\partial t} + \nabla \cdot (\rho \mathbf{v} r_t - K \nabla r_t) = \rho S_{cr} + \rho (S_{rs} - S_r) \quad (2)$$

Here,  $\rho$  is the density,  $\mathbf{v}$  is the velocity, and  $K$  is the eddy mixing coefficient.  $S_{es}$  is the source of equivalent potential temperature from surface fluxes;  $S_{er}$  is the source of  $\theta_e$  from radiation.  $S_{rs}$  is the source of total cloud water from surface evaporation;  $S_{cr}$  is minus the conversion rate of cloud water to precipitation.  $S_e$  and  $S_r$  are sinks of equivalent potential temperature and total water mixing ratio due to external sources; these are a consequence



of enforcing the WTG approximation. The domain mean potential temperature,  $\bar{\theta}$ , is relaxed to a reference profile representing the large scale,  $\theta_0$ . This relaxation is initiated by a potential temperature anomaly,  $(\bar{\theta} - \theta_0)$ , that accounts for radiative cooling and convective heating within the model domain. This modulates a potential temperature sink,  $S_\theta$ :

$$S_\theta = \lambda_\theta M(z)(\bar{\theta} - \theta_0) \quad . \quad (3)$$

Here  $1/\lambda_\theta$  is the time scale over which the domain mean potential temperature relaxes to the reference profile; physically it represents the time over which gravity waves would redistribute buoyancy anomalies.  $M(z) = \sin(\pi z/h)$  is a masking function which modulates the relaxation. It is applied only to the vertical layer  $b < z < h$ , where  $b$  is the height of the boundary layer top and  $h$  is the tropopause height. Above  $h$ ,  $M$  is set to zero. The temperature anomaly diagnosed in equation 3 then generates a vertical velocity that counteracts the heating via adiabatic cooling. This velocity is the weak temperature gradient vertical velocity,  $w_{wtg}$ , defined as:

$$w_{wtg} = \left( \frac{\partial \bar{\theta}}{\partial z} \right)^{-1} S_\theta \quad . \quad (4)$$

127 This parameterized vertical velocity vertically advects  $\theta_e$  and moisture. Since the WTG  
 128 vertical velocity is assumed to satisfy the anelastic mass continuity equation, vertical  
 129 motion can induce horizontal convergence of environmental air into the model domain.  
 130 This contributes to external sources,  $S_e$  and  $S_r$  in equations 1 and 2. The specific form  
 131 of these is given in section 3.3, where we discuss options for moisture treatment. In the  
 132 boundary layer, convective heating is shallow and the corresponding gravity waves are slow  
 133 [*Bretherton and Smolarkiewicz, 1989*]. Consequently, WTG is not a good approximation

134 for the boundary layer, so for  $z < b$  the WTG vertical velocity is linearly interpolated to  
135 zero from its value at  $b$ .

### 3. Numerical experiments

136 In this section, we describe the implementation of WTG in our model and the experi-  
137 ments used in this investigation.

#### 3.1. Model set-up

138 All numerical experiments in this study are conducted using two-dimensional geometry.  
139 The horizontal dimension is 200 km with 1 km grid resolution; the vertical spans 20 km  
140 with 250 m resolution. We choose to use two-dimensional domains for computational  
141 efficiency; previous studies have shown that they give qualitatively similar results as their  
142 three-dimensional counterparts [*Wang and Sobel, 2011*], and are therefore sufficient for  
143 this study.

144 All simulations use a uniform SST of 303 K. The model is run in non-WTG mode until  
145 the convective heating balances radiative cooling (radiative convective equilibrium, RCE).  
146 The RCE profiles are calculated with interactive radiation and a mean surface wind speed  
147 of  $5 \text{ ms}^{-1}$ . The strength of convection is modulated through surface fluxes which can  
148 be increased by increasing sea surface temperatures (SSTs) or surface wind speeds. To  
149 investigate the characteristics of convection in WTG mode, it is useful to increase the  
150 surface fluxes relative to the value used in the RCE calculation so the model exhibits  
151 stronger convective heating compared to radiative cooling. We choose to increase the  
152 surface wind speed to  $7 \text{ ms}^{-1}$  for most simulations, up to  $10 \text{ ms}^{-1}$  for multiple equilibria  
153 experiments (see below).

154 Although the RCE simulations invoke interactive radiation, we choose to perform all  
 155 WTG simulations with non-interactive (static) radiative cooling. The radiative cooling  
 156 profile is taken as the time and domain mean of the RCE simulation, see figure 1. Static  
 157 radiative cooling in the WTG simulations allows us to isolate the effect of changes in the  
 158 thermodynamic environment and moisture treatment independent of the changes to the  
 159 cooling profile that would occur with radiative feedbacks. Using the RCE cooling profile—  
 160 rather than a cooling profile that is held constant with height in the troposphere—allows  
 161 the convection to respond to a cooling profile that is more representative of the model  
 162 environment.

163 Finally, we must specify the time scale over which the domain averaged potential tem-  
 164 perature is relaxed to the reference profile ( $1/\lambda_\theta$  in equation 3).  $\lambda_\theta \rightarrow \infty$  represents  
 165 a strict enforcement of WTG ( $\bar{\theta} = \theta_0$ ), while  $\lambda_\theta \rightarrow 0$  turns WTG off and allows the  
 166 model to approach RCE. We choose a relaxation time scale of approximately 11 minutes  
 167 ( $\lambda_\theta = 1.5 \times 10^{-3} \text{ s}^{-1}$ ). Though this is too short to represent timescales of real physical  
 168 processes, it permits a larger range of parameters to exhibit multiple equilibria [*Sessions*  
 169 *et al.*, 2010], which we consider in this work.

### 3.2. Reference profiles

170 In the WTG approximation, we must specify reference profiles of potential temperature  
 171 and total water mixing ratio representative of the convective environment ( $\theta_0$  and  $r_{t0}$   
 172 in equations 3 and 6). The reference profiles are generated by running the model to  
 173 radiative convective equilibrium (RCE) in non-WTG mode (i.e.  $\lambda_\theta = 0$  in equation 3;  
 174 and  $\lambda_{hadv} = \lambda_m = 0$  in equation 6). Time and domain averages of potential temperature  
 175 and total water mixing ratio give the reference profiles  $\theta_0(z)$  and  $r_0(z)$ , shown in figure

176 2 for RCE simulations. The time average is taken over the last 30 days of a 1 year  
 177 simulation.

178 In order to investigate the response of convection to changes in the reference environ-  
 179 ment, we perform numerical experiments similar to *Raymond and Sessions* [2007]. *Ray-*  
 180 *mond and Sessions* [2007] showed that either moistening or stabilizing the environment  
 181 resulted in increased precipitation rates for given surface fluxes; increasing the reference  
 182 moisture increased the magnitude of the vertical mass flux without changing the shape,  
 183 while increasing the stability both increased the magnitude of the vertical mass flux and  
 184 lowered the level of maximum mass flux, resulting in more “bottom-heavy” convection.  
 185 As a consequence, this concentrates the convergence to low levels where the air is more  
 186 moist, resulting in a higher precipitation efficiency.

*Raymond and Sessions* [2007] represented changes to the reference environment by  
 adding idealized perturbations to either the potential temperature or the mixing ratio  
 reference profiles. An increase in the atmospheric stability was produced by specifying a  
 cooling of  $\delta\theta = 2$  K centered at  $h = 3$  km and a warming of the same magnitude centered  
 at  $h = 10$  km. The form of the perturbation centered at level  $h$  is given by:

$$\Delta\theta = \delta\theta \left(\frac{z}{h}\right)^2 e^{[2(1-z/h)]} \quad , \quad (5)$$

187 where  $z$  is the altitude. In addition to a more stable environment, we also explore the  
 188 impact of a less stable environment with perturbations of the same magnitude but with  
 189 opposite signs (warming of 2 K at 3 km with cooling of 2 K at 10 km).

190 Moistening or drying is achieved by modifying the reference mixing ratio profile with a  
 191 perturbation similar to equation 5, but with  $\delta\theta$  replaced by  $\delta r$ , where  $\delta r = \pm 1.0$  g kg<sup>-1</sup>  
 192 and  $h = 3$  km. This choice is consistent with the moisture perturbations of *Raymond and*

193 *Sessions* [2007], and is similar to the lower tropospheric drying level used in *Wang and*  
194 *Sobel* [2012]. In order to explore the full range of possible environments, we perform sets  
195 of nine experiments which account for all combinations of perturbations to the reference  
196 potential temperature and moisture profiles. These combinations are shown in figure 3.  
197 The symbols in the upper right corners of each panel represent the modifications to the  
198 reference profiles. Environmental stability is represented by the geometric stability of the  
199 symbols:

- 200 1. the completely unperturbed RCE profiles (control, center panel) are represented by  
201 a bulls-eye;
- 202 2. more stable environments (top row) are represented by upright triangles (geometri-  
203 cally more stable shapes);
- 204 3. less stable environments (bottom row) are represented by geometrically unstable,  
205 inverted triangles;
- 206 4. an atmosphere with the stability of the RCE profile is represented by a neutrally  
207 stable square (middle row).

208 The symbol shading indicates a moistening or drying of the reference environment. In  
209 analogy with a glass of water,

- 210 1. empty is drier;
- 211 2. half-filled is unperturbed;
- 212 3. filled is moister.

213 These symbols serve as a legend for results presented in section 5.

214 Rather than doing individual experiments for each combination shown in figure 3, ex-  
215 periments are run for 90 days with perturbations imposed in 30 day increments. For each

216 combination of perturbations, two sets of 90 day experiments are run; the first month is  
217 unperturbed; the second month has *either* potential temperature or moisture perturbed;  
218 the third month has *both* profiles perturbed. A set of eight experiments—graphically de-  
219 picted in figure 4—is required to represent all combinations of reference environments shown  
220 in figure 3.

221 The time-dependence in the experimental design has several advantages compared to  
222 individual experiments for each combination of perturbations:

223 1. It provides a minimum of two simulations with identical boundary conditions to  
224 confirm the uniqueness of the state for the given conditions (each combination of pertur-  
225 bations represented in figure 3 is repeated at least twice; the unperturbed reference state  
226 is repeated 8 times).

227 2. It confirms that the state in month 3 is unique as it is reached from two distinct  
228 steady states in the previous month;

229 3. It gives a sense of variability when conditions are the same;

230 4. It gives temporal information for studying the transition itself as the conditions  
231 change (though this is not explicitly studied in this paper).

232 We choose 30-day increments to give enough time for the system to re-equilibrate after  
233 the perturbation occurs, and enough simulation time to generate mean-state statistics.  
234 Statistics are taken from domain mean time averages over the last 2 weeks of each 30  
235 day run (minus one hour to avoid the ambiguous data at the transition). See figure 6  
236 in section 5 for sample data showing precipitation rate as a function of time for the 8  
237 experiments depicted in figure 4.

### 3.3. Moisture treatment

The prognostic equation for total water mixing ratio (equation 2) includes an external sink,  $S_r$ , which is a consequence of enforcing WTG. This external sink is given by

$$S_r = w_{wtg} \frac{\partial \bar{r}_t}{\partial z} + \lambda_{adv} (\bar{r}_t - r_x) \frac{1}{\rho_0} \frac{\partial \rho_0 w_{wtg}}{\partial z} + \lambda_m (\bar{r}_t - r_{t0}) \quad , \quad (6)$$

where

$$r_x = \begin{cases} \bar{r}_t & \text{if } \partial \rho_0 w_{wtg} / \partial z < 0 \quad (\text{detraining levels}) \\ r_{t0} & \text{if } \partial \rho_0 w_{wtg} / \partial z > 0 \quad (\text{entraining levels}) \end{cases} \quad . \quad (7)$$

238 The three terms on the right hand side of equation 6 represent sinks of moisture due  
 239 to large scale vertical advection by the mean vertical velocity  $w_{wtg}$ , explicit lateral en-  
 240 trainment from the surrounding environment, and an imposed relaxation to the reference  
 241 profile,  $r_{t0}$  which is independent of the WTG velocity.

242 As long as the model is operating in WTG mode,  $w_{wtg}$  is non-zero and moisture will be  
 243 vertically advected within the domain (first term, equation 6). Horizontal advection of  
 244 moisture occurs either by lateral entrainment due to divergent circulations generated by  
 245 enforcing mass continuity in the WTG velocity field (second term, equation 6), or from  
 246 large scale rotational flow that deposits dry or moist air into the domain independent of  
 247 WTG circulations. The latter is parameterized by relaxing the domain mean moisture  
 248 profile to the reference profile,  $r_{t0}$  (third term, equation 6). Figure 5 illustrates the  
 249 difference between these processes.

250 The choice of horizontal moisture advection scheme is set by the values of  $\lambda_{adv}$  and  $\lambda_m$ ,  
 251 which are specified externally.  $\lambda_{adv}$  has values of either 0 or 1, to turn lateral entrainment  
 252 off or on. Setting this to zero assumes the change in domain moisture via horizontal  
 253 advection is small compared to that due to the vertical advection; a value of 1 laterally

254 entrains moisture from the reference environment according to mass continuity of the  
255 WTG velocity field.  $\lambda_m = 0$  assumes horizontal moisture advection is purely divergent; a  
256 non-zero value relaxes the domain moisture to the reference profile over a timescale  $1/\lambda_m$ .  
257 Both of these choices have been employed in WTG experiments. *Raymond and Zeng*  
258 [2005]; *Raymond and Sessions* [2007]; *Sessions et al.* [2010]; *Wang et al.* [2013]; *Herman*  
259 *and Raymond* [2014] have all implemented explicit lateral entrainment of environmental  
260 moisture. Other investigations which explicitly aimed to determine the effect of moisture  
261 (including drying) on convection have relaxed moisture to a specified profile [*Sobel et al.*,  
262 2007; *Sobel and Bellon*, 2009; *Wang and Sobel*, 2012]. It is worth noting that *Sobel and*  
263 *Bretherton* [2000] investigated the effect of horizontal moisture advection by horizontal  
264 winds that were independent of WTG circulations; moisture relaxation parameterizes this  
265 mechanism.

266 Since the divergent and rotational flow are decoupled, both effects may influence convec-  
267 tion and we either choose one mechanism to represent the horizontal moisture advection,  
268 or we can simultaneously allow both to be turned on ( $\lambda_{adv} = 1$ ,  $\lambda_m \neq 0$ ) since both of  
269 these mechanisms may be at work in the real environment. In principle, the source due  
270 to large scale motions associated with the direct relaxation may have a unique reference  
271 profile that represents the moisture in an environment upstream from the convecting do-  
272 main. Since we do not have a reference profile to represent the upstream moisture, we  
273 simply assume that the reference profile represents the moisture immediately available to  
274 the convective domain, and we use this for both lateral entrainment and moisture relax-  
275 ation. Using this configuration, lateral entrainment and moisture relaxation will usually  
276 act in concert to either increase or decrease domain moisture, but in some conditions,



277 these mechanisms may compete and result in opposite tendencies (see section 5). In ei-  
278 ther case, when the WTG vertical velocity is zero or else implies divergence via equation  
279 7, the entrainment is shut off.

280 Alternatively, if we assume the horizontal contributions are small compared to the  
281 vertical advection of moisture, we can shut off both moisture schemes ( $\lambda_{adv} = 0$ ,  $\lambda_m = 0$ ).  
282 This is equivalent to an implicit horizontal moisture advection where moisture is advected  
283 into the domain via circulations that obey mass continuity, but they advect moisture  
284 from an environment that has a moisture profile identical to that in the model domain.  
285 The moisture profile of the domain is a result of a combination of surface evaporation,  
286 vertical advection by the WTG vertical velocity, and evaporation of precipitation, so in  
287 this case, the environmental moisture is determined by the modeled convection, and it is  
288 independent of an externally specified reference moisture profile. This has been a popular  
289 choice in previous studies [e.g., *Sobel and Bretherton*, 2000; *Sobel et al.*, 2007; *Wang and*  
290 *Sobel*, 2011; *Wang et al.*, 2013; *Anber et al.*, 2014]. Because this is the only moisture  
291 treatment which does not depend on a reference moisture profile, we refer to this as the  
292 control method.

293 For the simulations which include moisture relaxation, we choose a relaxation time scale  
294 of 1.8 days. To establish the moisture relaxation time scale, we conducted experiments  
295 over a range of moisture relaxation time scales and compared the modeled precipitation  
296 rate to the values produced using lateral moisture entrainment. Unperturbed environ-  
297 ments were not sensitive to the relaxation time chosen, but smaller relaxation times gave  
298 higher precipitation rates for more moist or more stable environments.  $1/\lambda_m = 1.8$  days  
299 represents the relaxation time that gives precipitation rates closest to those produced us-

ing lateral entrainment. It is important to note that strictly enforcing the moisture profile  
 (1/ $\lambda_m = 0$ ) shuts off the precipitation entirely because the reference profile is unsaturated  
 and thus cannot trigger rain production in our model.

*Wang and Sobel* [2012] performed a set of experiments that are similar to a subset  
 of the experiments presented here. In that work, the authors simulated the response of  
 convection to a layer of drying in the upper, middle, and lower troposphere. The drying  
 represented horizontal advection of dry air, and the layer was relaxed to a water vapor  
 mixing ratio of zero over a specified time scale. For drying perturbations applied to the  
 lower troposphere—at a level comparable to that used in this work—the moisture relaxation  
 time scale varied from 2.9 to 100 days, and they noted that time scales below this range  
 resulted in negative moisture values. The moisture relaxation time scale used in this work  
 is shorter—1.8 days—but we are imposing a much weaker drying (or moistening) than in  
*Wang and Sobel* [2012], and are thus far from this numerical limitation.

Since our prognostic variable is  $\theta_e$  rather than  $\theta$ , our choices of moisture treatment also  
 affect the sink of  $\theta_e$  (and consequently moist entropy, see discussion after equation 10):

$$S_e = w_{wtg} \frac{\partial \bar{\theta}_e}{\partial z} + \lambda_{hadv} (\bar{\theta}_e - \theta_x) \frac{1}{\rho_0} \frac{\partial \rho_0 w_{wtg}}{\partial z} + \lambda_m (\bar{\theta}_e - \theta_{e0}) \quad , \quad (8)$$

where the overbar indicates the domain mean,  $\theta_x$  is analogous to  $r_x$ , and  $\theta_{e0}$  is the reference  
 profile of equivalent potential temperature. Both  $\theta_0$  and  $r_{t0}$  (and thus  $\theta_{e0}$ ) can be functions  
 of time to permit study of convection in time-dependent situations.

### 3.4. Multiple equilibria

Multiple equilibria—steady states with either persistent precipitating deep convection or  
 a completely dry troposphere—exist in WTG simulations with identical boundary condi-

318 tions [Sobel *et al.*, 2007; Sessions *et al.*, 2010; Emanuel *et al.*, 2013; Herman and Raymond,  
319 2014]. If a set of parameters supports both equilibria, then whether the state is precipitat-  
320 ing or dry depends on the initial moisture of the troposphere. We perform several multiple  
321 equilibria experiments to determine how the existence of multiple equilibria depends on  
322 the thermodynamic environment ( $\theta_0(z)$ , equation 3;  $r_{t0}(z)$ , equations 6 and 7) and choice  
323 of moisture treatment.

324 As reported in Sessions *et al.* [2010], the model used here supports multiple equilibria  
325 for a range of wind speeds in conditions similar to those used in this work. Sessions  
326 *et al.* [2010] used unperturbed RCE reference profiles with laterally entrained moisture.  
327 A potentially significant difference, however, is that interactive radiation was used in the  
328 previous work; here, radiative cooling is static. Similar multiple equilibrium experiments  
329 were performed by Herman and Raymond [2014] on an updated version of this model with  
330 a modified WTG approach which spectrally decomposed the heating to accommodate  
331 gravity wave speeds representing a set of vertical modes. In a comparison of the “spectral  
332 WTG” approach with the conventional WTG (used in this study), multiple equilibria was  
333 found to exist only when conventional WTG was applied, and in that case, the range  
334 of multiple equilibria was sensitive to the choice of boundary layer height. We do not  
335 yet understand why conventional and spectral WTG give different results for multiple  
336 equilibria, though it may be related to the treatment of the boundary layer: in spectral  
337 WTG, convection confined to the boundary layer is shallow and thus has slow adjustment  
338 times [Bretherton and Smolarkiewicz, 1989]; in conventional WTG, this effect is artificially  
339 imposed via a linear interpolation of the WTG vertical velocity to zero in the boundary  
340 layer (see discussion after equation 4).

341 In another study, *Anber et al.* [submitted] compared the existence of multiple equilibria  
342 in WTG to an alternate parameterization of the large scale [damped gravity wave, DGW;  
343 see *Kuang, 2008; Blossey et al., 2009*, for a description]. In the parameter space they  
344 investigated, the WTG simulations exhibited multiple equilibria while DGW ones did not.  
345 Like spectral WTG, DGW does not require special treatment in the boundary layer, and  
346 the authors speculated that the existence of multiple equilibria may be an artifact of the  
347 boundary layer treatment when static radiation is used. Interactive radiation produced  
348 robust multiple equilibria in *Sessions et al.* [2010], so the role of radiation and boundary  
349 layer treatment is not entirely clear, and is left for future work.

350 The existence of multiple equilibria is sensitive to the method of parameterizing hori-  
351 zontal moisture advection. *Sobel et al.* [2007] demonstrated that multiple equilibria exist  
352 over a larger range of SSTs if horizontal moisture advection is not explicitly represented  
353 (equivalent to the control moisture treatment in this work) compared to when it is pa-  
354 rameterized by moisture relaxation (see their figure 2).

355 The first task is to determine whether multiple equilibria exist for an unperturbed en-  
356 vironment using different moisture treatments. To test this, we simply run an experiment  
357 with a surface wind speed of  $7 \text{ ms}^{-1}$  and with zero initial moisture in the domain. We  
358 do this for each moisture treatment to determine how different parameterizations of hori-  
359 zontal moisture advection affect the existence of multiple equilibria. As in *Sessions et al.*  
360 [2010], for all experiments which exhibit multiple equilibria, we repeat with a surface  
361 wind speed of  $10 \text{ ms}^{-1}$  to determine the range over which multiple equilibria exist. We  
362 also repeat with a more stable and more moist environment to determine the role of the  
363 thermodynamic environment on multiple equilibria.

#### 4. Diagnostics: characterizing convection and its environment

364 One of the most important measures of the strength of convection is the intensity of the  
 365 precipitation it produces. The precipitation rate in itself—especially when averaged over  
 366 space and time—is not enough to characterize the convection since different vertical and  
 367 horizontal arrangements can produce the same mean precipitation rate. In order to better  
 368 diagnose the convection, we compare the rain rates with several diagnostic quantities that  
 369 we describe below.

The environmental stability is characterized by an instability index,  $\Delta s^*$  [Raymond  
*et al.*, 2011; Gjorgjievska and Raymond, 2014], which is defined as

$$\Delta s^* = s_{low}^* - s_{high}^* \quad , \quad (9)$$

370 where  $s^*$  is the saturated moist entropy,  $s_{low}^*$  is the mean saturated moist entropy in the  
 371 level between 1 and 3 km, and  $s_{high}^*$  is the mean saturated moist entropy in the level  
 372 between 5 and 7 km. Since  $s^*$  is a function of temperature and pressure only, this charac-  
 373 terizes the stability of the environment: smaller values of the instability index correspond  
 374 to more stable environments; larger values characterize more unstable environments.

The moisture content of the domain is characterized by the saturation fraction, which  
 we approximate by

$$S = \frac{\int \rho(s - s_d) dz}{\int \rho(s^* - s_d) dz} \quad , \quad (10)$$

375 where the integrals are taken over the entire vertical depth of the model,  $s_d = c_p \ln(\theta/T_R)$   
 376 is the dry entropy ( $c_p = 1005 \text{ J kg}^{-1}\text{K}^{-1}$  is the specific heat at constant pressure, and  
 377  $T_R = 300 \text{ K}$  is a constant reference temperature), and  $s$  is the moist entropy (with  $\theta$   
 378 replaced by  $\theta_e$  in the dry entropy definition).

We define deep convective inhibition (DCIN) as a measure of how conducive or hostile the environment is to convection. As in *Raymond et al.* [2003],

$$DCIN = s_t^* - s_b \quad , \quad (11)$$

where the threshold entropy for convection,  $s_t^*$ , is the average saturated moist entropy over the layer at 1750-2000 m, and  $s_b$  is the boundary layer moist entropy, averaged over the lowest 1.75 kilometers of the domain. Smaller or negative values of DCIN are conducive to developing deep convection; larger values inhibit it.

The normalized gross moist stability (NGMS) provides a measure of the response of convection to its environment [*Neelin and Held*, 1987]. It is typically defined as the export of some quantity that is approximately conserved in moist processes (usually moist static energy or moist entropy) divided by some measure of the strength of the convection. As in *Raymond et al.* [2007], we choose NGMS ( $\Gamma$ ) to be the ratio of moist entropy import to moisture export:

$$\Gamma = \frac{T_R[\nabla_h \cdot (s\mathbf{v})]}{-L[\nabla_h \cdot (r\mathbf{v})]} = \frac{T_R \frac{1}{g} \int \nabla_h \cdot (s\mathbf{v}) dp}{-L \frac{1}{g} \int \nabla_h \cdot (r\mathbf{v}) dp} \quad . \quad (12)$$

The square brackets signify a vertical pressure integral over the troposphere,  $g$  is the gravitational acceleration, and  $\nabla_h$  is the horizontal divergence operator. The reference temperature,  $T_R$ , and latent heats of condensation plus freezing,  $L$  ( $L = 2.833 \times 10^6$  J  $\text{kg}^{-1}$ ), are included to make  $\Gamma$  dimensionless. Differing environmental profiles can significantly affect the value of  $\Gamma$ . Stabilizing or destabilizing the reference potential temperature will change the vertical profile of moist entropy which adjusts the lateral export of that quantity from the domain (numerator in equation 12); drying or moistening the environ-

ment clearly affects the import of moisture into the domain (denominator in equation 12),  
 but it can also affect the amount of moist entropy exported or imported at given levels.

It is useful to decompose the NGMS to isolate contributions due to horizontal and vertical transport. As in *Raymond and Fuchs* [2009] and *Raymond et al.* [2009], we use the identity

$$[\nabla_h \cdot (s\mathbf{v})] = [\mathbf{v} \cdot \nabla_h s] + [s\nabla_h \cdot \mathbf{v}] \quad , \quad (13)$$

anelastic mass continuity in pressure coordinates,

$$\nabla_h \cdot \mathbf{v} + \partial\omega/\partial p = 0 \quad , \quad (14)$$

where  $\omega$  is the vertical velocity in pressure coordinates, and integration by parts in pressure to obtain the relation

$$[s\nabla_h \cdot \mathbf{v}] = [\omega\partial s/\partial p] \quad . \quad (15)$$

Substituting this into equation 12 gives

$$\Gamma = \Gamma_h + \Gamma_v \quad , \quad (16)$$

where  $\Gamma_h = -T_R[\mathbf{v} \cdot \nabla_h s]/L[\nabla_h \cdot (r\mathbf{v})]$  and  $\Gamma_v = -T_R[\omega\partial s/\partial p]/L[\nabla_h \cdot (r\mathbf{v})]$ , the horizontal and vertical advection components, respectively. Often, the contribution due to horizontal advection is small compared to that from the vertical advection, and it can justifiably be neglected. In fact, in the original conception of gross moist stability, *Neelin and Held* [1987] neglected the horizontal contribution altogether, as have other since [e.g., *Yu et al.*, 1998]. However, in some cases, its contribution may be important.

Defining gross moist stability in terms of moist static energy, *Back and Bretherton* [2006] identified analogous contributions due to horizontal and vertical advection. They showed

400 that the horizontal advection of moist static energy was comparable to vertical advection  
 401 in rainy regions of the Pacific; they also found it could be negative. Vertical advection of  
 402 moist static energy was either negative (east Pacific) or positive (west Pacific), depending  
 403 on the vertical profile of vertical motion (which varied geographically). This has important  
 404 implications for the sign of gross moist stability.

In this work, we exclusively study the statistically steady state where NGMS is related to the net precipitation [precipitation,  $P$ , minus evaporation,  $E$ ; *Raymond et al.*, 2007]:

$$\Gamma = \frac{T_R(F_S - R)}{L(P - E)} . \quad (17)$$

405 Here,  $F_S$  is the surface moist entropy flux due to surface heat and moisture fluxes, and  $R$   
 406 is the pressure integral of the entropy sink per unit mass due to radiation divided by the  
 407 acceleration of gravity [*Raymond et al.*, 2007]. Most of the experiments described hold  
 408 the net entropy forcing constant: surface fluxes are fixed ( $F_S$  is constant) and a static  
 409 radiative cooling profile implies  $R$  is constant. Thus, we expect  $P - E \propto 1/\Gamma$ , where the  
 410 NGMS adjusts to account for the details of the thermodynamic environment.

We can infer much about the convective environment—as well as understand the relationship between our diagnostic quantities—by examining vertical profiles of mass flux,

$$\text{mass flux} = \rho w_{wtg} . \quad (18)$$

411 The vertical mass flux is calculated using the WTG vertical velocity. The total velocity  
 412 field is the sum of the explicit velocity calculated by the model and the velocity field  
 413 produced by enforcing WTG. Without WTG, mass conservation requires that the domain  
 414 mean vertical velocity be zero (what comes up must go down), so the only domain mean  
 415 vertical motion is that parameterized by the WTG approximation.



## 5. Results

416 In this section, we show the time evolution of precipitation and the diagnostic quantities  
 417 defined in section 4 to demonstrate the effect of changes in the thermodynamic environ-  
 418 ment. We also present vertical profiles of potential temperature and moisture anomalies  
 419 to compare with the imposed anomalies. Vertical profiles of mass flux demonstrate how  
 420 convection develops as a function of changes in the thermodynamic environment and pa-  
 421 rameterization of horizontal moisture advection. Finally, we compare steady state values  
 422 of precipitation and the diagnostic quantities defined in section 4 in a set of scatter-plots  
 423 to characterize the response of convection to changes in the large scale thermodynamic  
 424 environment.

### 5.1. Response to changes in the thermodynamic environment for laterally entrained moisture

425 Figure 6 shows a time series of the precipitation rate for the experiments outlined in  
 426 figure 4. For convenience, we only show the time series for moisture that is parameter-  
 427 ized by lateral entrainment ( $\lambda_{adv} = 1$ ,  $\lambda_m = 0$  in equation 6), similar results hold for  
 428 other moisture advection choices, but are not shown. All simulations use unperturbed  
 429 RCE profiles during the first month; each of the four panels represents the four possible  
 430 combinations of reference profiles when both  $\theta$  and  $r_t$  are perturbed; the second month  
 431 in each case represents either a drying/moistening OR a stabilizing/destabilizing. Each  
 432 case is marked with the symbol given in figure 3. Each distinct combination of reference  
 433 profiles (each panel in figure 3) is repeated at least twice (see figure 4). Statistics for  
 434 similar conditions are comparable, indicating statistically identical steady states.

435 For the perturbation magnitudes used in this study, atmospheric stability predominately  
436 affects the character of convection compared to atmospheric moisture. Specifically:

437 1. The increase in stability-cooling of 2 K at low levels and warming of 2 K aloft-  
438 produces a larger increase in precipitation rate ( $21 \text{ mm day}^{-1}$ ) than a  $1 \text{ g kg}^{-1}$  increase  
439 in atmospheric moisture of ( $12 \text{ mm day}^{-1}$ ); see the second month in figure 6a.

440 2. Decreasing the moisture by  $1 \text{ g kg}^{-1}$  at 3 km reduces-but does not shut off-the pre-  
441 cipitation; whereas destabilizing the environment completely shuts off the convection, even  
442 in a moister environment (compare empty squares in figure 6b,d with inverted triangles  
443 in figure 6c,d).

444 3. A drier, more stable environment increases the precipitation rate compared to the  
445 unperturbed RCE profile, whereas the moister, less stable environment is completely  
446 devoid of precipitation (compare the third month in figures 6b and 6c).

447 These observations are specific to the magnitudes of perturbations applied to the ref-  
448 erence profiles, though different choices would likely give qualitatively similar results. It  
449 would be interesting to investigate how different magnitudes of drying and moistening or  
450 stabilizing and destabilizing would affect the precipitation rate. *Wang and Sobel* [2012]  
451 performed a series of WTG experiments to see the effect that drying a layer would have on  
452 convection. In the lowest drying layer-comparable to the level that moisture perturbations  
453 are applied to in these experiments-relaxing the moisture to 0% relative humidity still  
454 produced convection with non-zero precipitation (though the convection became strictly  
455 shallow). Thus, we do not expect moisture perturbations to have as dramatic effects as  
456 perturbations in potential temperature.

457 In addition to precipitation rate, we consider several other diagnostic variables for char-  
458 acterizing convection and its environment. To develop some intuition about how these  
459 diagnostics behave for different convective environments, figure 7 shows time series of  
460 precipitation rate, saturation fraction, instability index, NGMS, and DCIN (these are all  
461 defined in section 4). The left column shows the results for the experiments which became  
462 more stable and more moist (experiments 1 and 2 in figure 4, figure 6a); while those on the  
463 right column evolve to less stable and drier states (experiments 7 and 8 in figure 4; figure  
464 6d). The vertical axes were chosen to be the same for both columns for easy comparison.  
465 All quantities were smoothed in time with a 1-day window. As in figure 6, horizontal  
466 moisture advection is parameterized using lateral entrainment.

467 From figure 7, we note several features of the diagnostic quantities. First, saturation  
468 fraction seems to adjust relatively quickly to changes in moisture and to an increase in  
469 stability, but it takes the domain a long time to adjust to a decrease in stability (figure 7d).  
470 The slow adjustment is primarily due to the relatively slow radiatively-driven subsidence  
471 rate, which determines the steady-state in absence of active convection. This only happens  
472 when horizontal moisture advection is parameterized using lateral entrainment for reasons  
473 described later in this section. Because we calculate mean quantities from the last two  
474 weeks of each month long segment, the long adjustment time for saturation fraction does  
475 not give the actual equilibrium value for the statistics calculated in this work. However, the  
476 error in the mean is much smaller than the difference between saturation fraction values  
477 for precipitating and non-precipitating states, so we simply make note of the difference  
478 and interpret the diagnostics accordingly.

479 The instability index—shown in figure 7e,f—is calculated from the saturated entropy.  
480 Since this is constrained by the enforcement of WTG, it quantifies “more stable” (small  
481 values) and “less stable” (large values) environments. It adjusts quickly to changes in  $\theta$   
482 profiles, but is not sensitive to changes in the reference moisture profile.

483 Depending on the atmospheric conditions, NGMS can be a highly variable quantity  
484 (figure 7g,h). It is defined as the ratio of lateral moist entropy export to lateral mois-  
485 ture import (equation 12). As convection evolves in the domain, these quantities can  
486 alternate between import and export. This is especially true if conditions are close to  
487 RCE: since the system is nearly in balance, there should be no net lateral import and  
488 export from the domain and these quantities alternate across the zero value. This results  
489 in large fluctuations, and in these conditions, NGMS is not a good diagnostic quantity.  
490 Because our simulations are performed in two-dimensions, there is more intermittency  
491 in convection which results in greater fluctuations between import and export compared  
492 to three dimensions [*Wang and Sobel, 2011*]. Even in a more stable environment (days  
493 30-60 in figure 7g) where moisture import exceeds export, convection is intermittent and  
494 significant fluctuations generate considerable variability in NGMS. On the other hand, for  
495 conditions which are not close to RCE—when either import or export is dominant—NGMS  
496 provides important information about the relationship between convection and the con-  
497 vective forcing. For example, the last month in figures 7g,h show steady, positive values  
498 of NGMS. In the more stable case with non-zero precipitation (figure 7g), the domain  
499 is importing moisture and exporting moist entropy, and the precipitation rate is related  
500 to the value of NGMS according to equation 17. In the less-stable environment (figure

7h), precipitation is suppressed, moisture is exported from the domain, and there is weak import of moist entropy. This is explained in more detail in section 5.3.

We can gain considerable insight to the response of convection to different thermodynamic environments by understanding the behavior of DCIN. Figure 7i,j shows the time evolution of DCIN, and figure 8 also shows the time series of the components of DCIN: the threshold saturated moist entropy ( $s_t^*$ ) is shown in red, the boundary layer moist entropy ( $s_b$ ) is in blue. These are plotted for the experiments where the  $\theta$  profile is perturbed first (solid lines in figure 8c,d), and the  $r_t$  profile is perturbed first (dotted line in figure 8e,f). There are three important observations:

1. Moisture perturbations have very little impact on either  $s_t^*$  or  $s_b$  (with the exception of increasing  $s_t^*$  in a more stable environment as seen at day 60 in figure 8C). This makes sense since  $s_t^*$  is a function only of temperature, and although WTG isn't directly enforced in the boundary layer,  $s_b$  is more sensitive to  $\theta_{ref}(z)$  than  $r_{t,ref}(z)$  (see figure 10); boundary layer moisture anomalies are fairly uniform in different moisture environments but are strong functions of stability. The boundary layer is drier in a more stable environment and moister in a less stable one.

2. Changing atmospheric stability affects both  $s_t^*$  and  $s_b$ , so the significant variations in DCIN are related to the direct change in  $s_t^*$  (which is calculated near the level of the perturbation) and an indirect change in moisture.

3.  $s_t^*$  and  $s_b$  rapidly adjust to changes in the reference profiles with one important exception: the boundary layer moist entropy,  $s_b$ , exhibits a very slow response to a decrease in atmospheric stability.

523 The last observation deserves some explanation. Recall that  $s_b$  is the mean moist entropy  
 524 in the lowest 1.75 km—which includes a thin layer just above the 1 km nominal boundary  
 525 layer. Immediately following the decrease in stability, DCIN increases trivially (figure 8b,  
 526 DCIN has a maximum of about  $5 \text{ J kg}^{-1}\text{K}^{-1}$  at day 30) as a result of the rapid increase  
 527 in  $s_t^*$  (the response time is less than a day, and is noted by the slight lead in increase in  $s_t^*$   
 528 compared to  $s_b$  at day 30 in figure 8d). After the initial increase, DCIN decreases sharply  
 529 over a period of about 3 days; boundary layer fluxes rapidly increase  $s_b$ . This is because  
 530 deep convection is suppressed due to the stable layer in the lower troposphere. Surface  
 531 fluxes eventually reach a steady state while radiatively-driven subsidence continues to  
 532 stifle convection of surface parcels and even acts to reduce boundary layer entropy. This  
 533 occurs over a period of about 25 days, after which DCIN finally reaches a steady state.  
 534 This mechanism also explains the gradual decline in saturation fraction in figure 7.

535 It is important to note that this slow response only occurs when lateral entrainment  
 536 is the choice for moisture treatment ( $\lambda_{adv} = 1$ ,  $\lambda_m = 0$ ); all other choices result in a  
 537 rapid adjustment to any change in the thermodynamic environment (not shown). The  
 538 long adjustment time for the lateral entrainment only treatment is likely a result of the  
 539 linear interpolation of the WTG vertical velocity to zero in the boundary layer (first two  
 540 terms in the right hand side of equations 6 and 8). This constraint implies that lateral  
 541 entrainment vanishes near the surface, so boundary layer entropy may only be reduced  
 542 by slower subsidence processes. When lateral entrainment is turned off ( $\lambda_{adv} = 0$ ), or  
 543 when other parameterizations of horizontal moisture advection are turned on ( $\lambda_m \neq 0$ ),  
 544 the boundary layer entropy can quickly adjust to the reference profile, thus reducing the  
 545 transition time.

## 5.2. Vertical profiles

546 In order to interpret the mean diagnostics, it is helpful to compare vertical profiles  
547 of  $\theta$  and  $r_t$  perturbations to the imposed perturbations; it is also useful to analyze the  
548 vertical motion that arises as a consequence of these anomalies and of the different param-  
549 eterizations for horizontal moisture advection. It is important to note that the vertical  
550 resolution throughout the troposphere—including the boundary layer—is 250 m. While this  
551 is sufficient for most of the troposphere, it is too coarse for the boundary layer and thus  
552 limits the extent to which we can make physical interpretations about the behavior in  
553 the boundary layer. Nevertheless, it is useful for making qualitative comparisons and  
554 explaining the response of convection to different thermodynamic environments.

555 As discussed in section 3.3, the choices for parameterizing horizontal moisture advection  
556 are entirely captured in the values for  $\lambda_{adv}$  and  $\lambda_m$  in equation 6. Lateral entrainment  
557 is either turned on or off ( $\lambda_{adv} = 1$  or  $\lambda_{adv} = 0$ ), while moisture relaxation is specified  
558 by the moisture relaxation rate,  $\lambda_m$  (where  $\lambda_m = 0$  means this mechanism is turned off).  
559 The choices are summarized in table 1, which also identifies the abbreviations used for  
560 the results of this section.

561 We expect the  $\theta$  profile to be very close to the reference profile—independent of the  
562 moisture treatment—simply as a consequence of enforcing the WTG approximation (see  
563 equation 3). Figure 9 shows that this is indeed the case: the model's  $\theta$  anomalies are  
564 very close to the imposed profiles, with the exception of the boundary layer where WTG  
565 is not enforced. The largest deviation from the free tropospheric reference profile occurs  
566 in the environment which is both moister and more stable (figure 9c); the domain mean

567 is slightly warmer in the lower troposphere, and the effect is slightly exaggerated in all  
568 cases where horizontal moisture advection is explicitly parameterized.

569 In contrast, there are significant differences in the moisture anomalies generated by the  
570 model compared to the imposed anomalies in the reference profile. A careful comparison  
571 of the moisture anomalies in figure 10 for each distinct environment suggests that the ref-  
572 erence moisture seems to play a supporting role for the convection rather than a dominant  
573 one. This is illustrated by noting that the shape of the moisture anomalies are more con-  
574 sistent with the perturbations applied to the  $\theta$  profiles than to the moisture profiles. For  
575 example, in the control case where moisture is only advected vertically ( $\lambda_{adv} = \lambda_m = 0$ ),  
576 there is no sensitivity to changes in the reference moisture profiles—by design—but there is  
577 dependence on the stability of the reference  $\theta$  profile. The stronger dependence on envi-  
578 ronmental stability is also seen when horizontal moisture advection is parameterized; for  
579 example, the top row of figure 10(a-c)—corresponding to more stable environments—shows  
580 more moist mid-tropospheres, even in a drier environment. In these cases, the lowest few  
581 kilometers are significantly drier, which is likely a consequence of weak descent in that  
582 layer (as seen in the vertical mass flux, figure 11a-c).

583 An important observation is that less stable environments (figure 10g-i) produce drier  
584 free tropospheres, even if the environment itself is moister (figure 10i). This is especially  
585 true if horizontal moisture advection is parameterized by lateral entrainment. In this  
586 case, radiatively driven subsidence and import of dry air at the entraining levels in the  
587 12-15 km layer in the upper troposphere (see figure 11g-i) results in an extremely dry  
588 anomaly—up to  $-9 \text{ g kg}^{-1}$ —at an altitude of 2 km. No other moisture treatment reduces  
589 the tropospheric moisture by this amount.



590 When used simultaneously, moisture relaxation and lateral entrainment usually work  
591 together to contribute either to an overall drying or moistening of the environment. An  
592 exception occurs in a less stable environment. In this case, lateral entrainment contributes  
593 to an extreme drying compared to the other parameterizations; when used in combination  
594 with moisture relaxation, the reference profile is moister than the domain mean vertical  
595 moisture profile, and the relaxation counters the extreme drying that occurs when lateral  
596 entrainment is used exclusively.

597 Comparing vertical mass flux profiles for the different moisture treatments in different  
598 environments can shed light on the behavior of convection in these simulations. With a few  
599 exceptions, the most important factor in determining the shape of the vertical mass flux  
600 profile is environmental stability. Changing the reference moisture primarily modulates  
601 the magnitude of the mass flux profile, but does not change the shape. This is in contrast  
602 to results presented by *Wang and Sobel* [2012] who found that extreme drying of a layer  
603 in the lower troposphere produced a more bottom heavy convective profile. It is possible  
604 that a larger magnitude of drying would do so here, but that study is outside the scope  
605 of this paper.

606 More stable environments—*independent of moisture or moisture treatment*—have  
607 stronger, more “bottom-heavy” convective profiles than unperturbed or less stable en-  
608 vironments (compare rows in figure 11). Buoyant parcels accelerate faster in the low-level  
609 cool anomaly, and become less buoyant in the warm anomaly aloft, thus producing a  
610 bottom-heavy profile. On the other hand, less stable environments inhibit convective de-  
611 velopment; consequently, radiative cooling produces subsidence throughout the free tropo-  
612 sphere, though weak updrafts persist in the boundary layer. Environments with decreased

613 stability effectively suppress convection— independent of the environmental moisture—with  
614 one exception: If horizontal moisture advection is turned off so that moisture transport  
615 within the domain is dominated by vertical advection (control case, black line), there is  
616 upward motion above 5 km, with slightly stronger descent between the boundary layer  
617 and 5 km. In this case, the cooling aloft accelerates the buoyant parcels upward while  
618 the warm anomaly below results in descent. This strict response to changes in the at-  
619 mospheric stability is modified significantly if horizontal moisture advection is explicitly  
620 parameterized and environmental moisture is permitted to enter the domain. In this  
621 case, drier environmental air (represented by the reference profile) inhibits condensation  
622 of lifted moisture—and evaporates any condensation—which cools the parcel and results in  
623 descent. The overturning of boundary layer air, necessitated by surface fluxes, is amplified  
624 by moister environmental air so this effect monotonically increases with the amplitude of  
625 the imposed moisture anomaly (figure 11g-i).

626 The most significant difference in mass flux profiles when comparing different parame-  
627 terizations of horizontal moisture advection occurs in less stable (non-precipitating) en-  
628 vironments: the mass flux profile differs significantly when horizontal advection is not  
629 explicitly parameterized (control) compared to when it is (via lateral entrainment and/or  
630 moisture relaxation). Aside from this, there aren't many significant qualitative differences  
631 in mass flux profiles for different moisture treatments with one exception: different mois-  
632 ture treatments do result in qualitatively different mass flux profiles with unperturbed  
633 stability (e.g., figure 11d). In the absence of  $\theta$ -perturbations, the convection is more  
634 sensitive to the choice for parameterizing moisture advection, especially in a dry environ-  
635 ment: there is almost no vertical motion if moisture relaxation is used (green line); weak

636 upward motion develops if moisture is laterally entrained (blue); but there is weak descent  
 637 if both mechanisms are employed (red). The moisture relaxation case is consistent with  
 638 the findings of *Wang and Sobel* [2012].

### 5.3. Diagnosing convection

639 Now that we have some insight as to how the shape and strength of convection de-  
 640 pends on atmospheric stability, environmental moisture, and choice for parameterizing  
 641 horizontal moisture advection, we investigate the relationship between precipitation and  
 642 the diagnostic quantities defined in section 4. This allows us to quantify the impact of  
 643 the thermodynamic environment on the convection itself. Figure 12 shows scatter plots  
 644 of rain as a function of saturation fraction, instability index, NGMS, and DCIN. Each  
 645 symbol represents time and domain averages of the last two weeks of each one month  
 646 segment of the simulations. The symbols themselves identify the reference environment–  
 647 the environmental moisture and stability–according to the legend embedded in the top  
 648 left panel (this symbol-only legend corresponds to the perturbations shown in figure 3).  
 649 Colors indicate moisture treatment used; table 1 gives a simple legend for abbreviations  
 650 and gives the values of  $\lambda_{adv}$  and  $\lambda_m$  which determine the moisture treatment according  
 651 to equation 6.

652 There are several observations to make from figure 12. First, consistent with observa-  
 653 tions [*Bretherton et al.*, 2004; *Peters and Neelin*, 2006; *Masunaga*, 2012; *Gjorgjievska and*  
 654 *Raymond*, 2014] and other modeling studies [*Derbyshire et al.*, 2004; *Sobel and Bellon*,  
 655 2009; *Wang and Sobel*, 2012], we see that precipitation is a strong function of saturation  
 656 fraction and instability index (figure 12a,b). More moist and more stable environments—as  
 657 indicated with smaller instability indices, higher saturation fractions, and filled upright

658 triangles—produce the highest precipitation rates. The former is expected; the latter is  
659 a consequence of the bottom-heavy convective profile associated with more stable envi-  
660 ronments (figure 11). The bottom-heavy convection vertically advects moister low level  
661 air which increases the precipitation efficiency, even in drier environments. This effect is  
662 enhanced in simulations with explicit lateral moisture entrainment ( $\lambda_{adv} = 1$ , blue and  
663 red symbols).

664 Less stable environments—as indicated with inverted triangles—inhibit precipitation in  
665 most cases (figure 12b; the exception being the control moisture treatment,  $\lambda_{adv} = \lambda_m =$   
666 0); they have lower saturation fractions and higher values of DCIN (figures 12a,d, re-  
667 spectively). The warm anomalies in the lower troposphere inhibit moist parcel ascent  
668 in general, and result in negative vertical mass fluxes throughout the troposphere. Note  
669 the extremely low saturation fractions observed with lateral entrainment (blue symbols  
670 in figure 12a). For this parameterization of horizontal moisture advection, very dry air  
671 enters the domain in the upper troposphere (above 12 km where  $\partial\rho_0 w_{wtg}/\partial z > 0$ ), where  
672 it is advected downwards and acts to inhibit convective development. This is further  
673 exacerbated by drying due to radiatively-driven subsidence down the moisture gradient,  
674 which severely dries the free troposphere (figure 10g-i). This has important consequences  
675 for multiple equilibria—and convective self-aggregation—as discussed in section 5.4.

676 There are a few cases where there is no precipitation despite having saturation fractions  
677 above 0.7; this occurs in a less stable environment when moisture relaxation is applied,  
678 either as the only treatment or in conjunction with lateral entrainment (figure 12a). In  
679 this case, moisture relaxation is moistening a 5 km layer above the surface (with heavy  
680 moistening in the boundary layer, see figure 10g-i) which results in a relatively high value

681 of saturation fraction. However, the temperature anomalies are still generating descent  
682 throughout the free troposphere which inhibits precipitation (compare mass flux profiles  
683 in figure 11h,i).

684 According to equation 17, static radiative cooling rates and fixed surfaces fluxes should  
685 produce an inversely proportional relationship between precipitation and NGMS. Figure  
686 12c demonstrates this beautifully for all moisture treatments with non-zero precipitation  
687 rates. We should note that NGMS is a poor diagnostic in conditions close to RCE since  
688 the system is nearly in balance and the net import/export of moisture and moist en-  
689 tropy is near zero, resulting in large variations in NGMS as a result of averaging zero  
690 over zero (in these simulations, values of NGMS  $> 1$  represent poor diagnostic values).  
691 Non-precipitating simulations all have small values of NGMS. In these cases, moisture is  
692 exported from the system while moist entropy is weakly imported due to circulations in  
693 the boundary layer. Note that there are several black symbols (control simulations) with  
694 negative values of NGMS. These simulations do not explicitly parameterize horizontal  
695 moisture advection ( $\lambda_{adv} = \lambda_m = 0$ )—the convection is insensitive to the reference mois-  
696 ture profile—and, as discussed in the previous section, they exhibit a drastically different  
697 convective profile compared to the other moisture treatments in unstable environments  
698 (figure 11g-i). Rather than descent through the entire free troposphere, there is ascent  
699 from 6 km to the tropopause which vertically advects moisture and produces a non-zero  
700 precipitation rate. In terms of the contribution to NGMS, however, the vertical motion  
701 in the lower troposphere— ascent in the boundary layer and descent between the top of the  
702 boundary layer and 5 km—gives net import (sources) of both moisture and moist entropy,  
703 which results in NGMS  $< 0$ .

704 More stable environments exhibit small or negative values of DCIN, and thus represent  
705 thermodynamic conditions most conducive for developing deep convection. We expect  
706 unstable environments to be associated with larger DCIN; this is the case for some exper-  
707 iments (figure 12d), though some show negative DCIN despite descent through the free  
708 troposphere (compare figure 11g-i). These cases have more moisture in the layer below  
709 1.75 km as a consequence of relaxing the domain mean moisture profile to the reference  
710 profile; this increases  $s_b$  and thus decreases DCIN in these cases.

711 It is interesting that the highest rainfall rates don't occur for the most negative values  
712 of DCIN, but rather for values that are near zero. We can understand this behavior by  
713 re-examining figures 7a,i and 8a,c. If the environment becomes more stable (e.g.,  
714 day 30 in 8c), both  $s_t^*$  and  $s_b$  decrease as a direct consequence of the applied cooling in  
715 the lower troposphere; this has a greater effect on  $s_t^*$ , which results in a negative DCIN  
716 (indicating an environment conducive to developing deep convection, see discussion in  
717 section 5.1). When moisture is then added to the lower troposphere (day 60 in figure 8c),  
718  $s_t^*$  increases slightly and DCIN becomes approximately zero (figures 8a,c and 12d). One  
719 possible explanation for the increase in  $s_t^*$  is that a more moist environment will entrain  
720 less dry air which results in less evaporative cooling, and a slightly higher temperature. In  
721 contrast, a drier environment will experience more evaporative cooling and more negative  
722 DCIN values (compare empty and filled upright triangles in figure 12d). Since DCIN is  
723 approximately equal to negative lower tropospheric convective available potential energy  
724 (CAPE), dry parcels require more negative values of DCIN to ascend.

725 We can further understand the factors controlling the characteristics of convection by  
726 considering relationships between the diagnostic quantities themselves. Figure 13 shows  
727 scatter plots which compare saturation fraction, instability index, NGMS, and DCIN.

728 Figure 13a clearly demonstrates that the more stable the environment, the higher the  
729 saturation fraction [this is consistent with results of *Gjorgjievska and Raymond, 2014*]. For  
730 a given reference moisture profile (denoted by line style), the relationship is nearly linear  
731 for most moisture treatments. The exception to this is the extreme drying in unstable  
732 environments when horizontal moisture advection is parameterized by lateral entrainment.  
733 This reinforces the notion that the important difference between moisture treatments  
734 is not what happens when it is raining (precipitation rates and mass flux profiles are  
735 fairly consistent), but what happens to the domain when it is not raining. This may be  
736 especially relevant for interpreting results of WTG simulations which impose observed data  
737 in time-dependent reference profiles, or for understanding conditions permitting multiple  
738 equilibria.

739 Figure 13b shows the relationship between saturation fraction and NGMS. For precip-  
740 itating environments in conditions where NGMS is a good diagnostic, smaller values of  
741 NGMS correlate to larger saturation fractions (see inset, figure 13b), which is consistent  
742 with the rain-NGMS relation of figure 12. In non-precipitating cases, NGMS is small as  
743 a consequence of weak import (or export) of moist entropy near the top of the boundary  
744 layer.

745 There is not a significant relationship between NGMS and DCIN (figure 13c). This is an  
746 interesting result that is consistent with the theories posited by *Raymond and Fuchs* [2007]  
747 and *Raymond and Fuchs* [2009]. Together, these papers developed a highly simplified

748 model of the interaction between the large scale and tropical oceanic convection. Their  
749 analytic model identifies two types of convectively coupled waves: moisture modes in which  
750 convection acts to increase—rather than decrease—the saturation fraction (this happens  
751 when NGMS is negative), and another mode which is destabilized by convective inhibition.  
752 An example of the latter is convectively coupled Kelvin waves, and recent modeling results  
753 by *Fuchs et al.* [2014] demonstrated the role of DCIN in destabilizing the two-dimensional  
754 analog of convectively coupled Kelvin waves. This simplified picture suggests that either  
755 NGMS or DCIN is the control for destabilizing the environment, depending on the nature  
756 of the interaction between convection and the large scale. In reality, the dynamic processes  
757 are much more complicated due to the inherent nonlinearity of the atmosphere, so we  
758 do not expect an obvious relation between NGMS and DCIN, despite good correlations  
759 between other convective diagnostics.

760 Similarly, there is also no obvious overall correlation between DCIN and saturation  
761 fraction (figure 13d). Here, the primary observation is that more stable environments—  
762 upright triangles—experience small or negative DCIN, which is indicative of an environment  
763 conducive to convection. As explained above, DCIN in these environments becomes less  
764 negative for more moist environments (indicated with filled upright triangles and higher  
765 saturation fractions) because less dry air is entrained, evaporative cooling is diminished,  
766 and the threshold entropy increases. Also noteworthy is that the highest values of DCIN  
767 accompany the lowest saturation fractions, and these occur only with laterally entrained  
768 moisture, and only in the most hostile environment for convection: more unstable and  
769 drier.

770 To summarize figures 12 and 13, we note the following features:



771 1. The precipitation rate is highly sensitive to both the saturation fraction and the  
772 atmospheric stability (as measured by the instability index).

773 2. Stable environments are conducive to precipitating states: they are moist, sport  
774 small or negative values of DCIN, and give the highest precipitation rates.

775 3. Environmental moisture serves to modulate the precipitation by entraining more or  
776 less moisture as available, but in the current implementation of WTG, it doesn't seem to  
777 overcome the atmospheric stability. In other words,

778 (i) Unstable environments have greatly diminished moisture and precipitation; moist-  
779 ening the environment doesn't change this.

780 (ii) More stable environments are very conducive to precipitation. Drying the envi-  
781 ronment reduces—but does not eliminate—the precipitation in the domain.

782 4. NGMS—which summarizes our ignorance about the relationship between convection  
783 and the convective forcing—is strongly related to the precipitation rate. In the steady state  
784 with approximately constant entropy forcing, we expect—and we observe—an inversely pro-  
785 portional relationship between precipitation rate and NGMS in precipitating states. The  
786 relationship between NGMS and other diagnostics, however, is not as straight-forward:

787 (i) There is only a slight direct dependence of NGMS on atmospheric stability, which  
788 is stronger for moister environments and nearly absent for drier environments. Most likely,  
789 the biggest impact of atmospheric stability is an indirect result of modifying the vertical  
790 mass flux profile which controls lateral entrainment and detrainment of moist entropy and  
791 moisture.

792 (ii) For the precipitating states, and for environments which are sufficiently different  
793 from RCE, there is an inverse relation between NGMS and saturation fraction. Dry states,  
794 on the other hand, all seem to exhibit small and sometimes negative values of NGMS [in  
795 agreement with *Sessions et al.*, 2010].

#### 5.4. Multiple Equilibria

796 One important application of WTG experiments relates to the analogy between the  
797 smaller domain WTG simulations which exhibit multiple equilibria—either a persistent  
798 precipitating steady state or a completely dry subsiding troposphere—and the dry and  
799 moist regions of a larger domain RCE simulation with self-aggregated convection. Thus,  
800 we consider the effect of different reference environments and moisture treatments on  
801 multiple equilibria. Insight in this context may help elucidate the behavior of convection  
802 in self-aggregation simulations.

803 Whether or not a particular set of conditions exhibit multiple equilibria is determined  
804 by performing a set of parallel experiments in which all parameters are identical with  
805 the exception of the initial tropospheric moisture content: one experiment is initialized  
806 with the reference moisture profile, while the other is initially completely dry. If the  
807 initially moist experiment maintains persistent precipitating convection while the initially  
808 dry experiment remains dry with zero precipitation, then the set of parameters exhibits  
809 multiple equilibria. If, on the other hand, the initially dry profile develops precipitating  
810 convection—or if the initially moist profile evolves to and maintains a dry steady state—then  
811 there is a single equilibrium. We hypothesize that parameters which affect the existence  
812 of multiple equilibria in WTG experiments are also important for self-aggregation in large  
813 RCE simulations.

814 As demonstrated in *Sessions et al.* [2010], the model used in this experiment supports  
815 multiple equilibria in conditions similar to those used in this work. Using lateral entrain-  
816 ment of moisture and interactive radiation, *Sessions et al.* [2010] found multiple equilibria  
817 to exist for a significant range of wind speeds with unperturbed RCE reference profiles. In  
818 an updated version of the model, *Herman and Raymond* [2014] showed multiple equilibria  
819 occurs with static, non-interactive radiation (though not when a spectral form of WTG  
820 is implemented).

821 The first task is to determine whether the existence of multiple equilibria in this model  
822 depends on the parameterization of horizontal moisture advection. *Sobel et al.* [2007]  
823 demonstrated that states of multiple equilibria are sensitive to how moisture advection  
824 is parameterized; here we test this systematically with different horizontal moisture ad-  
825 vection treatments. Specifically, we run experiments initialized with zero tropospheric  
826 moisture, using unperturbed reference profiles, for each moisture treatment. All other  
827 parameters are identical to the experiments reported in previous sections (including sur-  
828 face wind speeds of  $7 \text{ ms}^{-1}$ ). Of all the moisture treatments, the only one to maintain a  
829 dry equilibrium state over 30 days was lateral moisture entrainment ( $\lambda_{hadv} = 1$ ,  $\lambda_m = 0$ ).  
830 That multiple equilibria exist for lateral entrainment in these experiments is undoubtedly  
831 a consequence of the extreme drying of the free troposphere that only occurs with this  
832 choice (figure 10g-i). The extreme drying is conducive to maintaining a dry state and  
833 supporting multiple equilibria. These results are summarized in table 2.

834 To determine how robust multiple equilibria are with laterally entrained moisture, we  
835 repeated the experiment with zero initial tropospheric moisture, but with a surface wind  
836 speed of  $10 \text{ ms}^{-1}$ . In this case, the experiment began to precipitate and only a single

837 equilibrium state exists. This is an important result: with static radiative cooling, multiple  
838 equilibria exists over a range of wind speeds from 5-10  $\text{ms}^{-1}$  only if horizontal moisture  
839 advection is parameterized with lateral entrainment. Figure 14 shows the precipitation  
840 rate for the multiple equilibria experiments performed with laterally entrained moisture.

841 The results of this section are consistent with the multiple equilibria results of *Sobel*  
842 *et al.* [2007] and *Herman and Raymond* [2014]. *Sobel et al.* [2007] found that parameter-  
843 izing large scale moisture advection via a moisture relaxation reduced the range of SSTs  
844 which permitted multiple equilibria compared to experiments that did not explicitly pa-  
845 rameterize horizontal moisture advection (similar to our control method). *Herman and*  
846 *Raymond* [2014] tested multiple equilibria in the conventional WTG (as in this work) and  
847 in a version of WTG which spectrally decomposes heating (with lateral entrainment and  
848 static radiation). It is important to note that in the results of *Herman and Raymond*  
849 [2014], their model only exhibited multiple equilibria for the conventional WTG approach  
850 (as used in this work), but not in the spectrally modified implementation, and further-  
851 more, multiple equilibria depended on the height of the boundary layer. The existence of  
852 multiple equilibria may also depend on many other model details, including domain size  
853 or the degree to which WTG is enforced [*Sessions et al.*, 2010], details of the implemen-  
854 tation of WTG [e.g., *Daleu et al.*, 2012], or background SST [*Emanuel et al.*, 2013]. How  
855 each of these factors affects the existence of multiple equilibria is not fully understood;  
856 experiments such as this are aimed to improve the overall understanding, and especially  
857 determine which factors are representative of physical processes in the atmosphere.

858 Finally, to determine the sensitivity of multiple equilibria to changes in environmental  
859 stability and moisture, we performed two more experiments with lateral moisture entrain-

860 ment and an initially dry troposphere: the first in a more stable environment, the second  
861 in a more moist environment. In both cases, the model produced precipitating convection  
862 and multiple equilibria were not sustained.

## 6. Summary

863 We used a cloud system resolving model on a two-dimensional domain with the large  
864 scale parameterized by the weak temperature gradient (WTG) approximation to inves-  
865 tigate the response of convection to changes in the thermodynamic environment. The  
866 thermodynamic environment was initially set by vertical profiles of potential temperature  
867 and moisture in radiative convective equilibrium (RCE), and we added perturbations to  
868 change the environmental stability and moisture. For the magnitudes of perturbations  
869 explored in this work, we found that atmospheric stability dominates changes in the char-  
870 acter of convection by prescribing the vertical motion in the domain:

- 871 1. more stable environments produce bottom heavy convection with higher precipita-  
872 tion rates than unperturbed profiles—even in drier environments.
- 873 2. less stable environments shut off precipitation by generating descent throughout the  
874 free troposphere.

875 On the other hand, the environmental moisture modulates precipitation rates according  
876 to the amount of moisture available for precipitation—they can amplify or weaken vertical  
877 motion—but in general they don't change the shape of the convective profile.

878 Convection is characterized by a set of diagnostics that includes precipitation rate,  
879 vertical mass flux, an instability index (a measure of instability), saturation fraction,  
880 normalized gross moist stability (NGMS), and deep convective inhibition (DCIN). The  
881 shape of the vertical mass flux directly affects budgets of moisture and moist entropy in

882 the domain, which sets the values of the diagnostic quantities. Our results show that in  
883 environments which support precipitating convection, the precipitation rate is a sensitive  
884 function of saturation fraction, and is inversely proportional to NGMS. Atmospheric sta-  
885 bility also plays an important role in the relationship between diagnostics: more stable  
886 environments—characterized by smaller instability indices—correlate with higher satura-  
887 tion fractions. These relationships hold independent of the perturbations applied to the  
888 reference environments.

889 Horizontal moisture advection plays an important role in the interaction between con-  
890 vection and the large scale circulations. We investigate alternate parameterizations of  
891 this process, which include lateral entrainment by divergent circulations induced by en-  
892 forcing WTG, a moisture relaxation which represents a parameterization of horizontal  
893 moisture advection by non-divergent circulations, a combination of both of these, and  
894 control simulations which assume horizontal advection is negligible compared to vertical  
895 advection (so lateral entrainment and moisture relaxation are both turned off). In ther-  
896 modynamic environments which support precipitating convection, there is little difference  
897 in the characteristics of convection—as determined by precipitation rate, saturation frac-  
898 tion, DCIN, NGMS and vertical profiles of mass flux—for different moisture treatments  
899 (except that precipitation rate is insensitive to changes in reference moisture if horizontal  
900 moisture advection is not explicitly parameterized via lateral entrainment or a relaxation  
901 to a reference profile). The most significant difference between moisture treatments is  
902 seen when the environment does not support convection (less stable environments). The  
903 most significant effects are:

904 1. A drastic decrease in free tropospheric moisture when horizontal moisture advection  
905 is parameterized by lateral entrainment.

906 2. If both lateral entrainment and moisture relaxation are turned off—so the domain  
907 is not sensitive to changes in environmental moisture—the model generates ascent in the  
908 upper troposphere which supports light precipitation. In this case, moisture and moist  
909 entropy are both imported, and NGMS is negative.

910 Multiple equilibria—dry or precipitating states in identical boundary conditions—are of  
911 particular interest because of the hypothesized relationship to dry and moist regions in  
912 larger domain RCE simulations where convection has self-aggregated. In this work, we  
913 investigated the sensitivity of multiple equilibria to changes in the thermodynamic envi-  
914 ronment and different parameterizations of horizontal moisture advection. Using static  
915 (non-interactive) radiative cooling, we found that the existence of multiple equilibria is  
916 sensitive to both the thermodynamic environment and choice of moisture treatment. For  
917 the parameters used in this work, our model only exhibited multiple equilibria for laterally  
918 entrained moisture in an unperturbed reference environment. Other moisture treatments  
919 exhibited only a single equilibrium, and imposing either a more stable or more moist  
920 environment destroyed the dry equilibrium state even when moisture was laterally en-  
921 trained. To the extent that multiple equilibria are analogous to dry and moist regions in  
922 a self-aggregated RCE simulation—and to the extent that the MJO can be depicted as a  
923 manifestation of self-aggregation—these results may be significant for improving simula-  
924 tions of the MJO [*Pritchard and Bretherton, 2014; Zhu and Hendon, 2015*].

925 Our results are important not only for understanding the physics of tropical convec-  
926 tion, but also for interpreting other studies which implement WTG. As far as mechanisms

927 governing the development of deep convection, our results suggest that convection is very  
928 sensitive to the thermodynamic environment. Other large scale forcing mechanisms, in-  
929 cluding radiative cooling, surface fluxes, or the propagation of atmospheric waves, may  
930 affect convection indirectly by modifying the thermodynamic environment. For example,  
931 easterly waves generate virtual temperature anomalies—similar to those idealized in this  
932 work—that enhance or suppress convection [*Reed and Recker, 1971; Raymond and Ses-*  
933 *sions, 2007; Gjorgjievska and Raymond, 2014*]. We are not suggesting that there are no  
934 direct influences on convection by these mechanisms, only that this work provides strong  
935 evidence that there is also an indirect effect which acts via a modification of the ther-  
936 modynamic environment. This is significant insight given the growing use of the WTG  
937 approximation to understand different aspects of tropical convection, including tropical  
938 cyclogenesis [*Raymond and Sessions, 2007*] and the Madden-Julian Oscillation [*Wang*  
939 *et al., 2013*].

940 **Acknowledgments.** We thank David Raymond, Adam Sobel, Shuguang Wang,  
941 George Craig, and Saska Gjorgjievska for helpful discussions. This work was supported  
942 by U.S. National Science Foundation Grants AGS-1056254, ATM-1021049, and AGS-  
943 1342001. Data used for this research are available upon request from the corresponding  
944 author; please send requests via email to [sessions@kestrel.nmt.edu](mailto:sessions@kestrel.nmt.edu). The model used to  
945 generate the data is available at <http://kestrel.nmt.edu/~raymond/tools.html>.

## References

946 Anber, U., S. Wang, and A. Sobel (2014), Response of atmospheric convection to vertical  
947 wind shear: Cloud-system-resolving simulations with parameterized large-scale circula-



948 tion. part i: Specified radiative cooling, *J. Atmos. Sci.*, *71*, 2976–2993, doi:10.1175/JAS-  
949 D-13-0320.1.

950 Back, L. E., and C. S. Bretherton (2006), Geographic variability in the export of moist  
951 static energy and vertical motion profiles in the tropical pacific, *Geophys. Res. Lett.*,  
952 *33*, L17810, doi:10.1029/2006GL026672.

953 Blossey, P. N., C. S. Bretherton, and M. C. Wyant (2009), Subtropical low cloud re-  
954 sponse to a warmer climate in a superparameterized climate model. part ii: Col-  
955 umn modeling with a cloud resolving model, *J. Adv. Model. Earth. Syst.*, *01*, 8, doi:  
956 10.3894/JAMES.2009.1.8.

957 Bretherton, C. S., and P. K. Smolarkiewicz (1989), Gravity waves, compensating subsi-  
958 dence and detrainment around cumulus clouds, *J. Atmos. Sci.*, *46*, 740–759.

959 Bretherton, C. S., T. Uttal, C. W. Fairall, S. E. Yuter, R. A. Weller, D. Baumgardner,  
960 K. Comstock, R. Wood, and G. B. Raga (2004), The EPIC 2001 stratocumulus study,  
961 *Bull. Am. Meteor. Soc.*, *85*, 967–977.

962 Bretherton, C. S., P. N. Blossey, and M. Khairoutdivnov (2005), An energy-balance analy-  
963 sis of deep convective self-aggregation above uniform sst, *J. Atmos. Sci.*, *62*, 4273–4292.

964 Daleu, C. L., S. J. Woolnough, and R. S. Plant (2012), Cloud-resolving model simulations  
965 with one- and two-way couplings via the weak temperature gradient approximation, *J.*  
966 *Atmos. Sci.*, *69*, 3683–3699, doi:10.1175/JAS-D-12-058.1.

967 Derbyshire, S. H., I. Beau, P. Bechtold, J.-Y. Grandpeix, J.-M. Piriou, J.-L. Redelsperger,  
968 and P. M. M. Soares (2004), Sensitivity of moist convection to environmental humidity,  
969 *Q. J. R. Meteorol. Soc.*, *130*, 3055–3079, doi:10.1256/qj.03.130.

- 970 Emanuel, K., A. A. Wing, and E. M. Vincent (2013), Radiative-convective instability, *J.*  
971 *Adv. Model. Earth Syst.*, *5*, doi:10.1002/2013MS000270.
- 972 Fuchs, Z., S. L. Sessions, and D. J. Raymond (2014), Mechanisms controlling the  
973 onset of simulated convectively coupled kelvin waves, *Tellus A*, *66*, 22107, doi:  
974 10.3402/tellusa/v.66.22107.
- 975 Gjorgjievska, S., and D. J. Raymond (2014), Interaction between dynamics and ther-  
976 modynamics during tropical cyclogenesis, *Atmos. Chem. Phys.*, *14*, 3065–3082, doi:  
977 10.5194/acp-14-3065-2014.
- 978 Herman, M. J., and D. J. Raymond (2014), Wtg cloud modeling with spectral decompo-  
979 sition of heating, *J. Adv. Model. Earth Syst.*, *06*, doi:10.1002/2014MS000359.
- 980 Jeevanjee, N., and D. M. Romps (2013), Convective self-aggregation, cold pools, and  
981 domain size, *Geophys. Res. Lett.*, *40*, 1–5, doi:10.1002/grl.50204.
- 982 Kuang, Z. (2008), Modeling the interaction between cumulus convection and linear gravity  
983 waves using a limited-domain cloud system-resolving model, *J. Atmos. Sci.*, *65*, 576–  
984 591.
- 985 Kuang, Z. (2010), Linear response functions of a cumulus ensemble to temperature and  
986 moisture perturbations and implications for the dynamics of convectively coupled waves,  
987 *J. Atmos. Sci.*, *67*, 941–962, doi:10.1175/2009JAS3260.1.
- 988 Mapes, B. E. (2004), Sensitivites of cumulus-ensemble rainfall in a cloud-resolving model  
989 with parameterized large-scale dynamics, *J. Atmos. Sci.*, *61*, 2308–2317.
- 990 Masunaga, H. (2012), Short-term versus climatological relationship between precipitation  
991 and tropospheric humidity, *J. Climate*, *25*, 7983–7990, doi:10.1175/JCLI-D-12-00037.1.

- 992 Muller, C. J., and I. M. Held (2012), Detailed investigation of the self-aggregation of con-  
993 vection in cloud-resolving simulations, *J. Atmos. Sci.*, *69*, 2551–2565, doi:10.1175/JAS-  
994 D-11-0257.1.
- 995 Neelin, J. D., and I. M. Held (1987), Modeling tropical convergence based on the moist  
996 static energy budget, *Mon. Weat. Rev.*, *115*, 3–12.
- 997 Peters, O., and J. D. Neelin (2006), Critical phenomena in atmospheric precipitation, *Nat.*  
998 *Phys.*, *2*, 393–396, doi:10.1038/nphys314.
- 999 Pritchard, M. S., and C. S. Bretherton (2014), Causal evidence that rotational moisture  
1000 advection is critical to the superparameterized madden-julian oscillation, *J. Atmos. Sci.*,  
1001 *71*, 800–815, doi:10.1175/JAS-D-13-0119.1.
- 1002 Raymond, D. J., and Z. Fuchs (2007), Convectively coupled gravity and moisture  
1003 modes in a simple atmospheric model, *Tellus*, *59A*, 627–640, doi:10.1111/j.1600-  
1004 0870.2007.00268.x.
- 1005 Raymond, D. J., and Z. Fuchs (2009), Moisture modes and the madden-julian oscillation,  
1006 *J. Climate*, *22*, 3031–3046, doi:10.1175/2008JCLI2739.1.
- 1007 Raymond, D. J., and S. L. Sessions (2007), Evolution of convection during tropical cyclo-  
1008 genesis, *Geophys. Res. Lett.*, *34*, L06,811, doi:10.1029/2006GL028607.
- 1009 Raymond, D. J., and X. Zeng (2005), Modelling tropical atmospheric convection in the  
1010 context of the weak temperature gradient approximation, *Quart. J. Roy. Meteor. Soc.*,  
1011 *131*, 1301–1320.
- 1012 Raymond, D. J., G. B. Raga, C. S. Bretherton, J. Molinari, C. López-Carrillo, and Z. Fuchs  
1013 (2003), Convective forcing in the intertropical convergence zone of the eastern Pacific,  
1014 *J. Atmos. Sci.*, *60*, 2064–2082.

- 1015 Raymond, D. J., S. L. Sessions, and Z. Fuchs (2007), A theory for the spinup of tropical  
1016 depressions, *Q. J. Roy. Meteor. Soc.*, *133*, 1743–1754.
- 1017 Raymond, D. J., S. L. Sessions, A. H. Sobel, and Z. Fuchs (2009), The mechanics of gross  
1018 moist stability, *J. Adv. Model. Earth Syst.*, *1*, 9, doi:10.3894/JAMES.2009.1.9.
- 1019 Raymond, D. J., S. L. Sessions, and C. L. Carrillo (2011), Thermodynamics of trop-  
1020 ical cyclogenesis in the northwest Pacific, *J. Geophys. Res.*, *116*, D18,101, doi:  
1021 10.1029/2011JD015624.
- 1022 Reed, R. J., and E. E. Recker (1971), Structure and properties of synoptic-scale wave  
1023 disturbances in the equatorial western pacific, *J. Atmos. Sci.*, *28*, 1117–1133.
- 1024 Sessions, S. L., S. Sugaya, D. J. Raymond, and A. H. Sobel (2010), Multiple equilibria in a  
1025 cloud resolving model using the weak temperature gradient approximation, *J. Geophys.*  
1026 *Res.*, *115*, D12110, doi:10.1029/2009JD013376.
- 1027 Sobel, A. H., and G. Bellon (2009), The effect of imposed drying on parameterized deep  
1028 convection, *J. Atmos. Sci.*, *66*, 2085–2096, doi:10.1175/2008JAS2926.1.
- 1029 Sobel, A. H., and C. S. Bretherton (2000), Modeling tropical precipitation in a single  
1030 column, *J. Climate*, *13*, 4378–4392.
- 1031 Sobel, A. H., G. Bellon, and J. Bacmeister (2007), Multiple equilibria in a single-  
1032 column model of the tropical atmosphere, *Geophys. Res. Lett.*, *34*, L22,804, doi:  
1033 10.1029/2007GL031320.
- 1034 Tulich, S. N., and B. E. Mapes (2010), Transient environmental sensitivities of explicitly  
1035 simulated tropical convection, *J. Atmos. Sci.*, *67*, 923–940, doi:10.1175/2009JAS3277.1.
- 1036 Wang, S., and A. H. Sobel (2011), Response of convection to relative sea surface temper-  
1037 ature: cloud-resolving simulations in two and three dimensions, *J. Geophys. Res.*, *116*,

1038 D11,119, doi:10.1029/2010JD015347.

1039 Wang, S., and A. H. Sobel (2012), Impact of imposed drying on deep convection in a  
1040 cloud-resolving model, *J. Geophys. Res.*, *117*, D02112, doi:10.1029/2011JD016847.

1041 Wang, S., A. H. Sobel, and Z. Kuang (2013), Cloud-resolving simulation of TOGA-  
1042 COARE using parameterized large scale dynamics, *J. Geophys. Res.*, *118*, 6290–6301,  
1043 doi:10.1002/jgrd.50510.

1044 Wing, A. A., and K. A. Emanuel (2013), Physical mechanisms controlling self-aggregation  
1045 of convection in idealized numerical modeling simulations, *J. Adv. Mod. Earth Sys.*, *5*,  
1046 1–14, doi:10.1002/2013MS000269.

1047 Yu, J.-Y., C. Chou, and J. D. Neelin (1998), Estimating the gross moist stability of the  
1048 tropical atmosphere, *J. Atmos. Sci.*, *55*, 1354–1372.

1049 Zhu, H., and H. H. Hendon (2015), Role of large-scale moisture advection for simulation  
1050 of the mjo with increased entrainment, *Q. J. R. Meteorol. Soc.*, doi:10.1002/qj.2510.

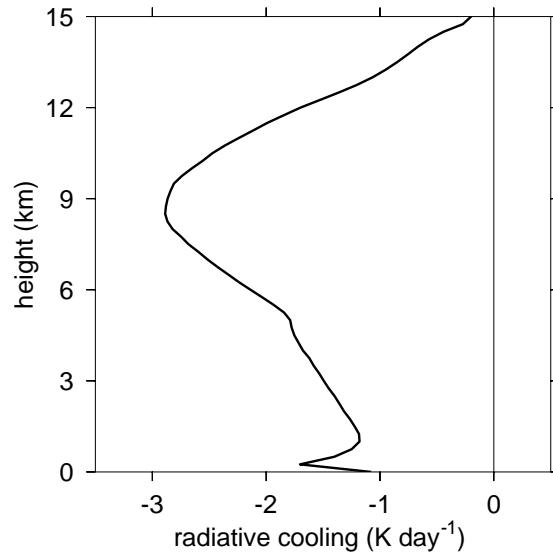


**Figure 1.** Mean radiative cooling profile from a radiative convective equilibrium (RCE) simulation. This cooling profile is the prescribed static cooling for all experiments in this work.

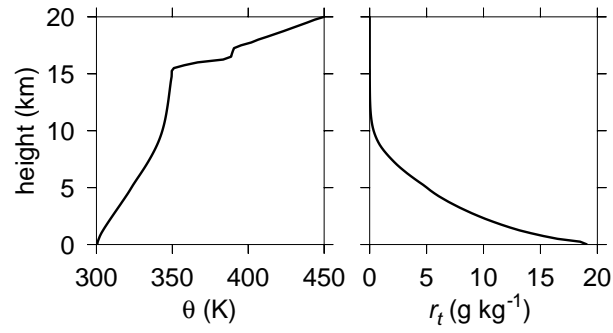


**Figure 2.** Radiative convective equilibrium (RCE) profiles of potential temperature (left) and total water mixing ratio (right) used as unperturbed reference profiles in WTG calculations. RCE is calculated over a uniform SST of 303 K, with surface wind speed of  $5 \text{ ms}^{-1}$  and interactive radiation on a 2D, 200 km horizontal domain.

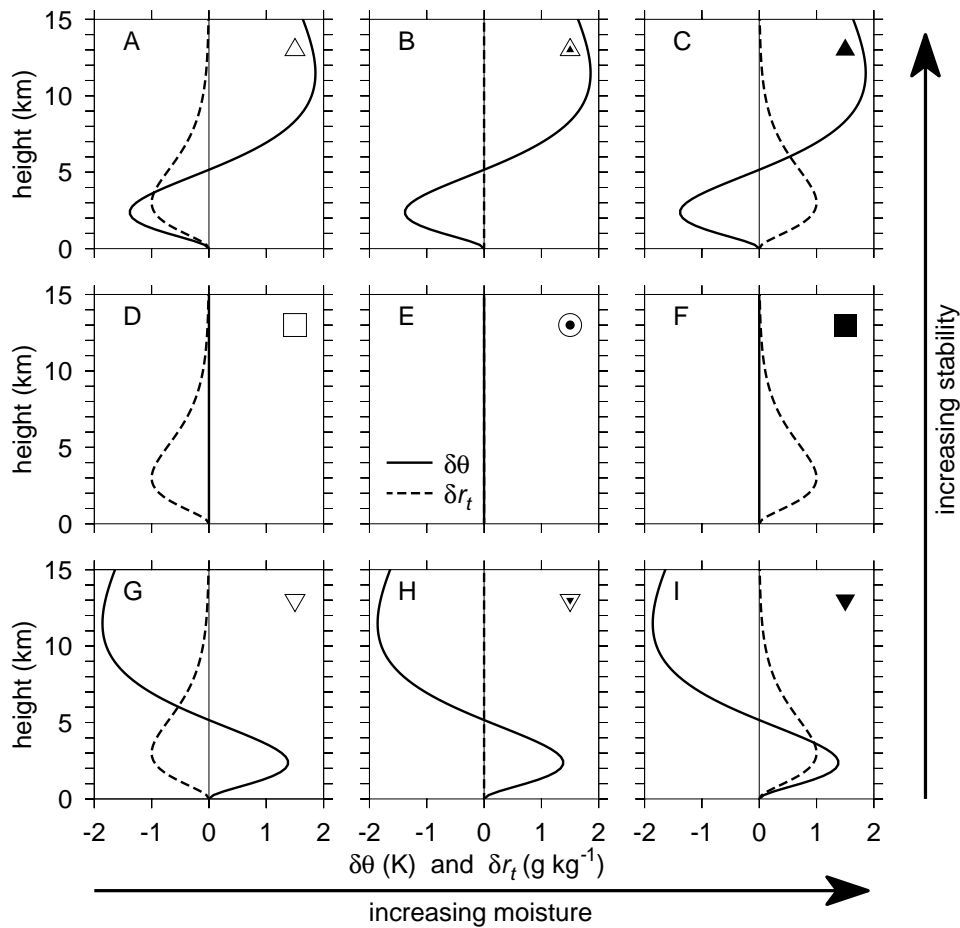


**Figure 3.** Perturbations added to the RCE reference profile. Solid lines represent perturbations to the potential temperature profiles, dashed lines give mixing ratio perturbations. The center panel is the unperturbed RCE reference state. The middle row has unperturbed reference potential temperature profiles, the top row has perturbations representing more stable environments, the bottom row represents less stable environments. Similarly, the middle column has no perturbations added to the reference moisture environment, the left column is drier, the right column, moister. The symbols in the upper right of each panel represent the reference environment. The shading represents the moisture perturbation: empty symbols are drier, full symbols are moister, half-filled symbols have unperturbed moisture profiles. The squares are unperturbed  $\theta$  profiles; more stable environments are represented by upright triangles (geometrically more stable shapes); less stable environments are represented by inverted triangles. In order to easily distinguish the unperturbed RCE profiles, we choose bulls-eyes to represent these simulations. This figure serves as a symbol legend for results presented in section 5.



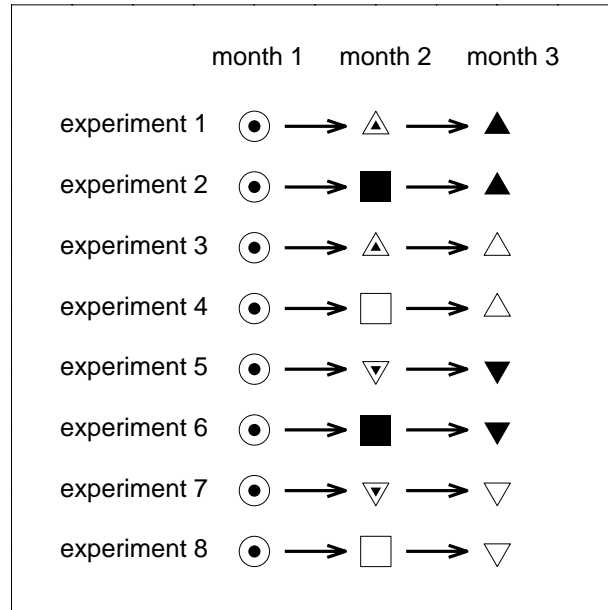


**Figure 4.** Graphic showing the sequence of perturbations applied in each experiment.

Symbols are the same as in figure 3: bulls-eyes are unperturbed profiles; squares indicate no change in stability; triangles indicate change in stability (upright are more stable); amount of filling represents environmental moisture perturbation with empty being drier and filled being moister.

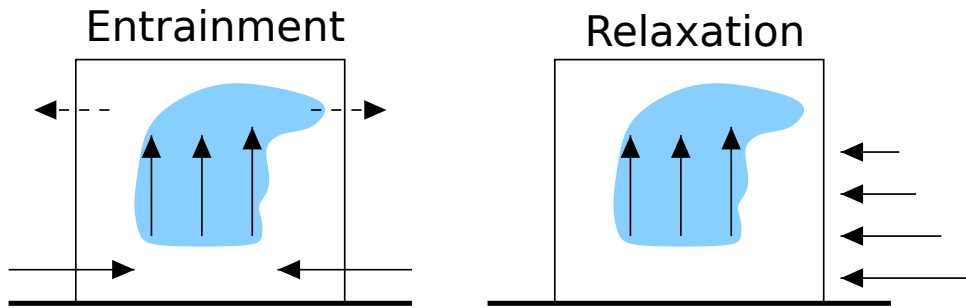


**Figure 5.** Cartoon representations of the physical processes captured by the different parameterizations of horizontal moisture advection. In each case, the box represents the domain of the CRM. Arrows pointing up represent the WTG vertical mass flux ( $\rho w_{wtg}$ ). The outside of each box represents the environment and therefore the reference profiles used in the WTG experiments. The left panel shows the lateral entrainment of the reference moisture at low levels which results from convergence via mass continuity in the WTG velocity field. The dashed arrows indicate the detrainment that would occur in the real atmosphere due to divergence in a layer where buoyancy decreases with height. Since detrainment of intrinsic quantities doesn't alter the modeled environment, there is no change in the moisture due to this mechanism (see equation 7). The right panel illustrates how moisture might enter the domain from large scale circulations that are independent of those induced by WTG; this process is parameterized by directly relaxing the domain mean moisture profile to the reference profile.

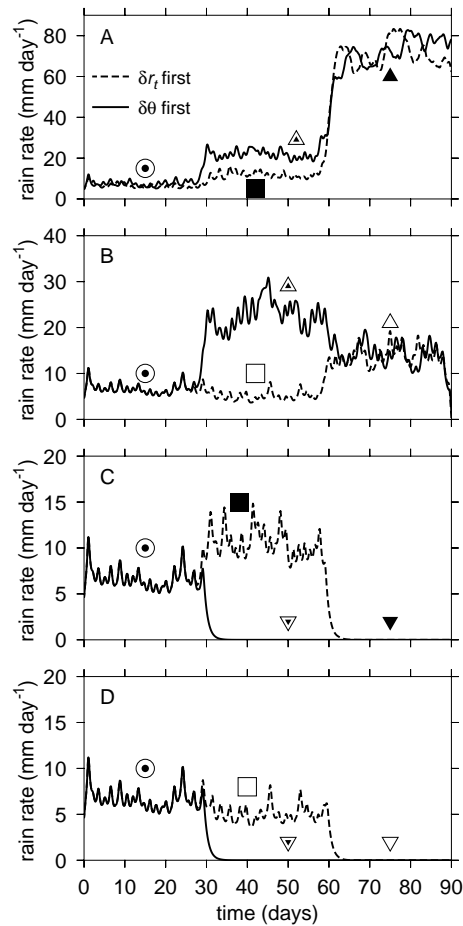


**Figure 6.** Three month time series of precipitation for the eight WTG experiments graphically described in figure 4. a) Experiments 1 and 2; b) experiments 3 and 4; c) experiments 5 and 6; d) experiments 7 and 8. The symbols indicate the perturbations of the reference profile for the one month segment, the symbol legend is given in figure 3. Solid and dashed lines indicate whether the reference  $\theta$  or reference  $r_t$  profiles, respectively, were perturbed first (these indicate the perturbed profile during the second month of the experiments).

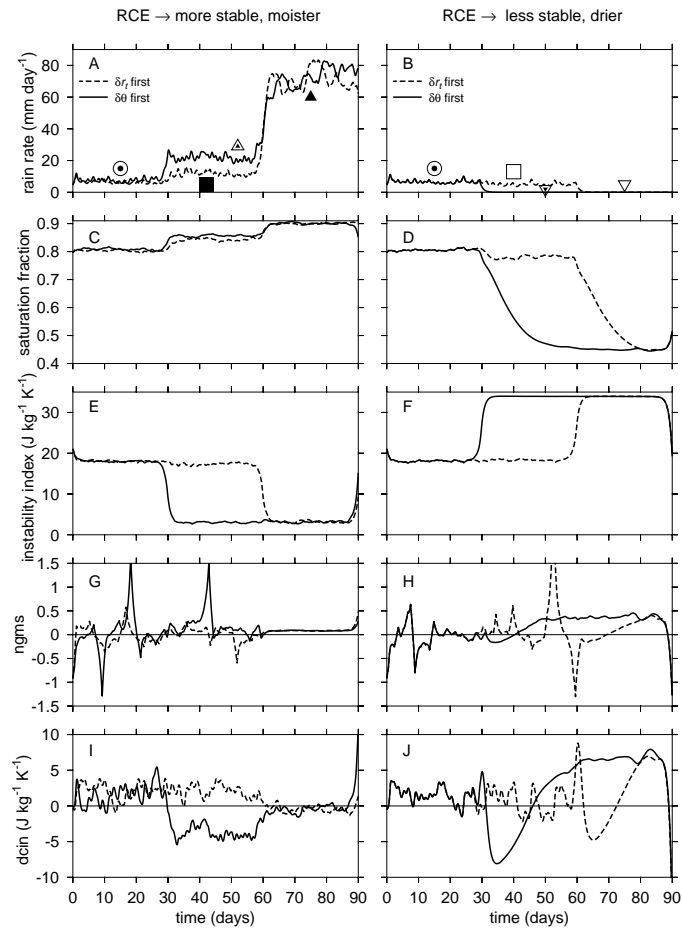


**Figure 7.** Time series showing rain rate (a,b), saturation fraction (c,d), instability index (e,f), NGMS (g,h), and DCIN (i,j) for experiments which became more stable and moister (left column, experiments 1 and 2 in figure 4), and those which became less stable and drier (right column, experiments 7 and 8 in figure 4).

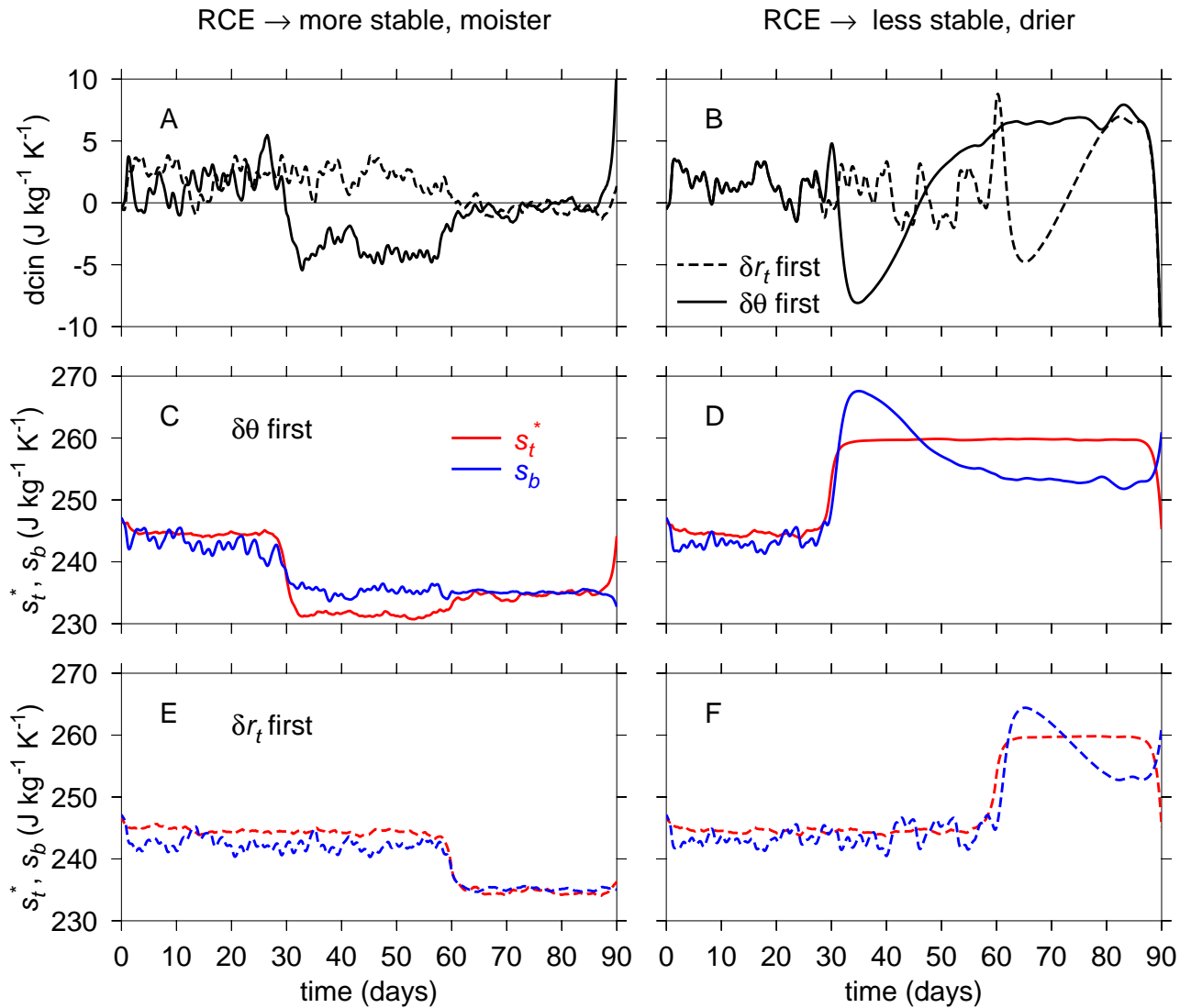


**Figure 8.** Time series of DCIN (a,b), and DCIN components,  $s_t^*$  and  $s_b$  (c-f). The solid lines represent experiments where the  $\theta$  profile was perturbed first (c,d), while dashed lines represent experiments where moisture perturbations are imposed first (e,f). As in figure 7, the left column represents experiments 1 and 2 while the right column shows results for experiments 7 and 8 (see figure 4).

	$\lambda_{hadv} = 0$	$\lambda_{hadv} = 1$
$\lambda_m = 0$	control	lat ent
$\lambda_m = 1/1.8 \text{ days}^{-1}$	m-relax	both

**Table 1.** Abbreviations for the different combinations of moisture treatment. The values of  $\lambda_{hadv}$  and  $\lambda_m$  (equation 6) determine the choice for parameterizing horizontal moisture advection. This is the key for identifying each method: lateral entrainment (lat ent), moisture relaxation (m relax), both (lat ent & m relax). Choosing  $\lambda_{hadv} = \lambda_m = 0$  disconnects the modeled convection from the reference moisture profile; this is the control.

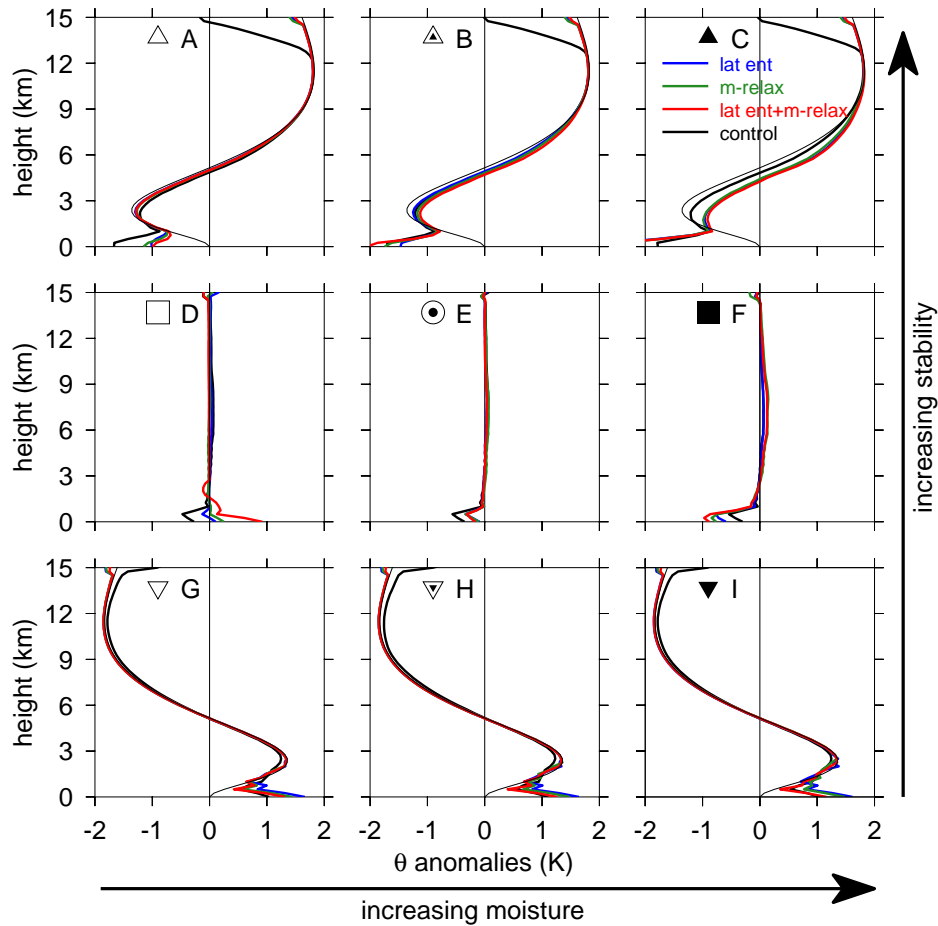


**Figure 9.** Modeled  $\theta$  anomalies for each distinct thermodynamic environment (represented symbolically as in figure 3). Colors represent moisture treatment: lateral entrainment is blue; moisture relaxation is green; red uses both lateral entrainment and moisture relaxation; black uses neither. For reference, the thin black lines show the anomalies imposed on the reference profile (see figure 3).

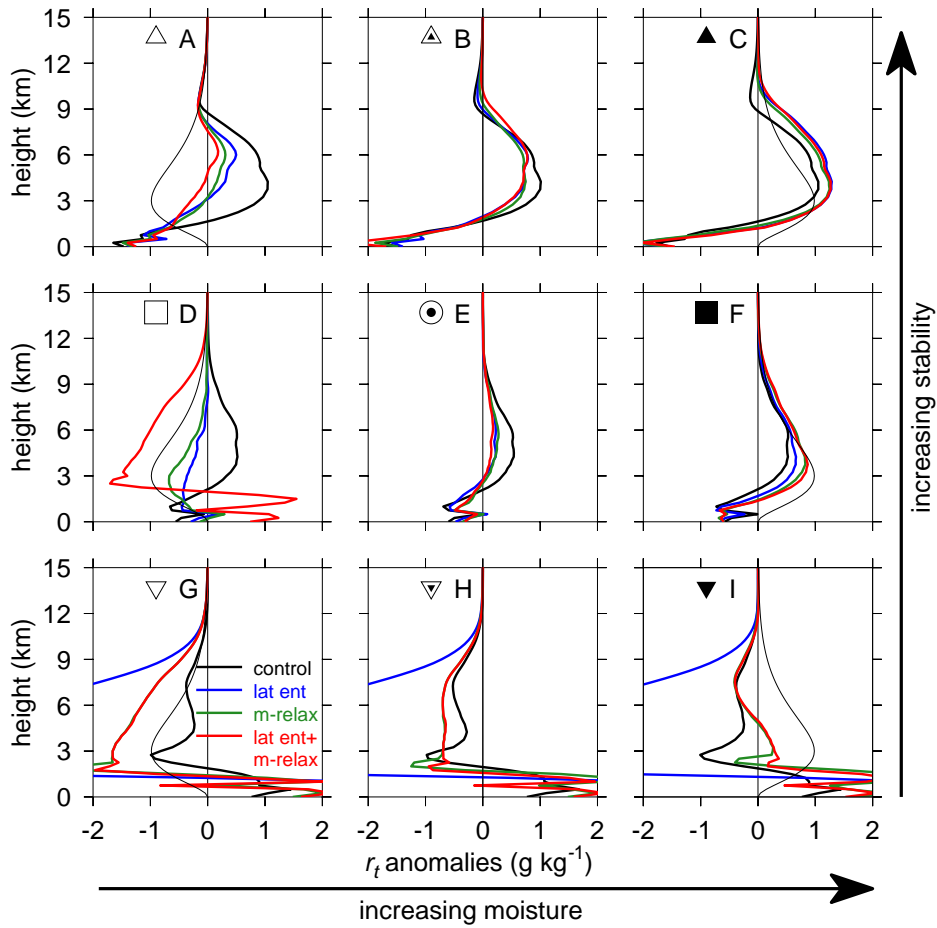


**Figure 10.** Moisture anomalies for different thermodynamic environments using different moisture treatments (denoted by color; see table 1 for a legend of abbreviations). The thin black line shows the imposed moisture perturbation for reference (same as figure 3). The dry anomaly for lateral entrainment (blue) in panels g-i has a minimum value of nearly  $-9 \text{ g kg}^{-1}$  at an altitude of about 2 km.



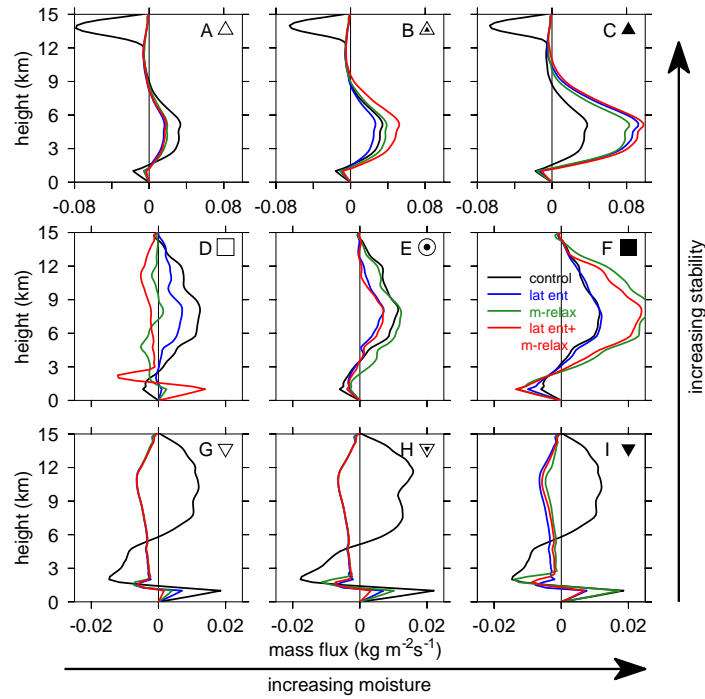


**Figure 11.** Vertical profiles of vertical mass flux (equation 18) for each environmental profile. Colors represent the moisture treatment used. Note the different horizontal scale in the top row figures compared to the other rows. Each tick mark on the horizontal axes in the top row represents  $0.04 \text{ kg m}^{-2}\text{s}^{-1}$ , while those in the middle and bottom rows represent  $0.02 \text{ kg m}^{-2}\text{s}^{-1}$ . More stable environments exhibit much stronger vertical mass fluxes.

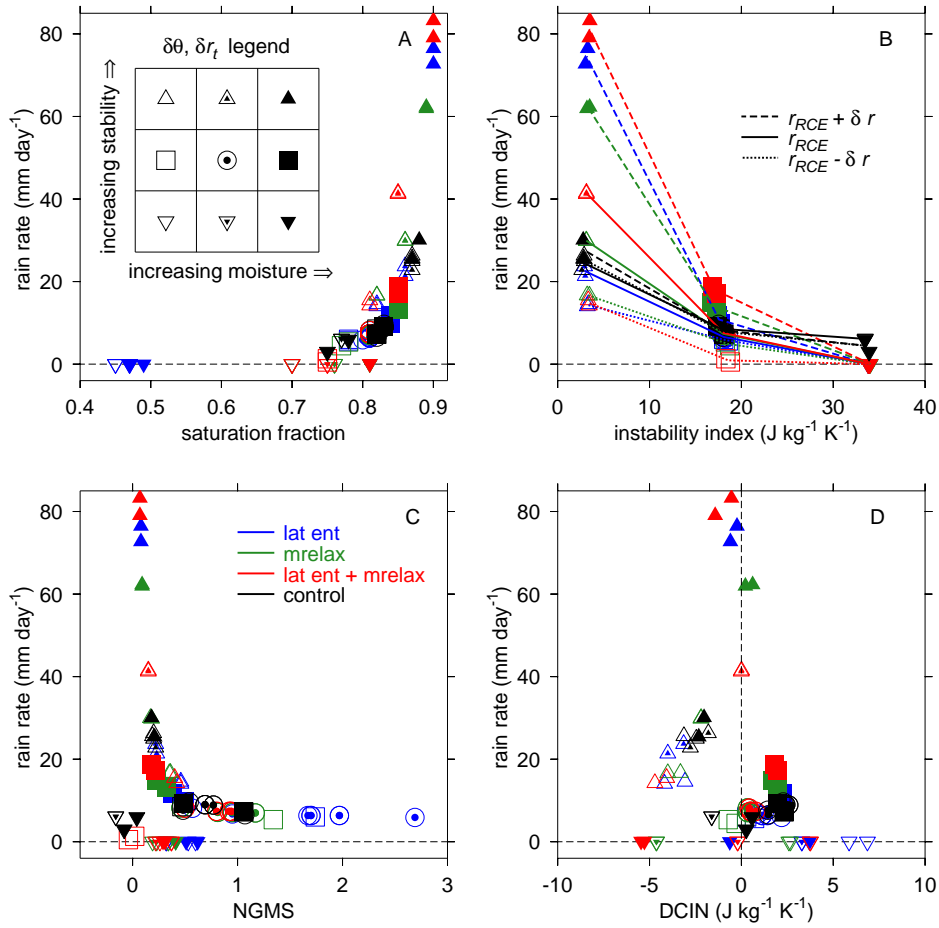


**Figure 12.** Scatterplots of precipitation as a function of (a) saturation fraction, (b) instability index, (c) NGMS, and (d) DCIN. Each shape represents a domain and time average for a given set of environmental conditions (see legend inset in panel a, and corresponding perturbations in figure 3). Colors represent parameterization choices for horizontal moisture advection according to table 1: blue indicates explicit lateral entrainment; green is moisture relaxation; red indicates both are used, and black is the control (no explicit parameterization). The lines in panel (b) connect experiments with identical reference moisture profiles: solid lines have unperturbed moisture profiles ( $r_{RCE}$ ), dashed are more moist ( $r_{RCE} + \delta r$ ), dotted are drier ( $r_{RCE} - \delta r$ ).

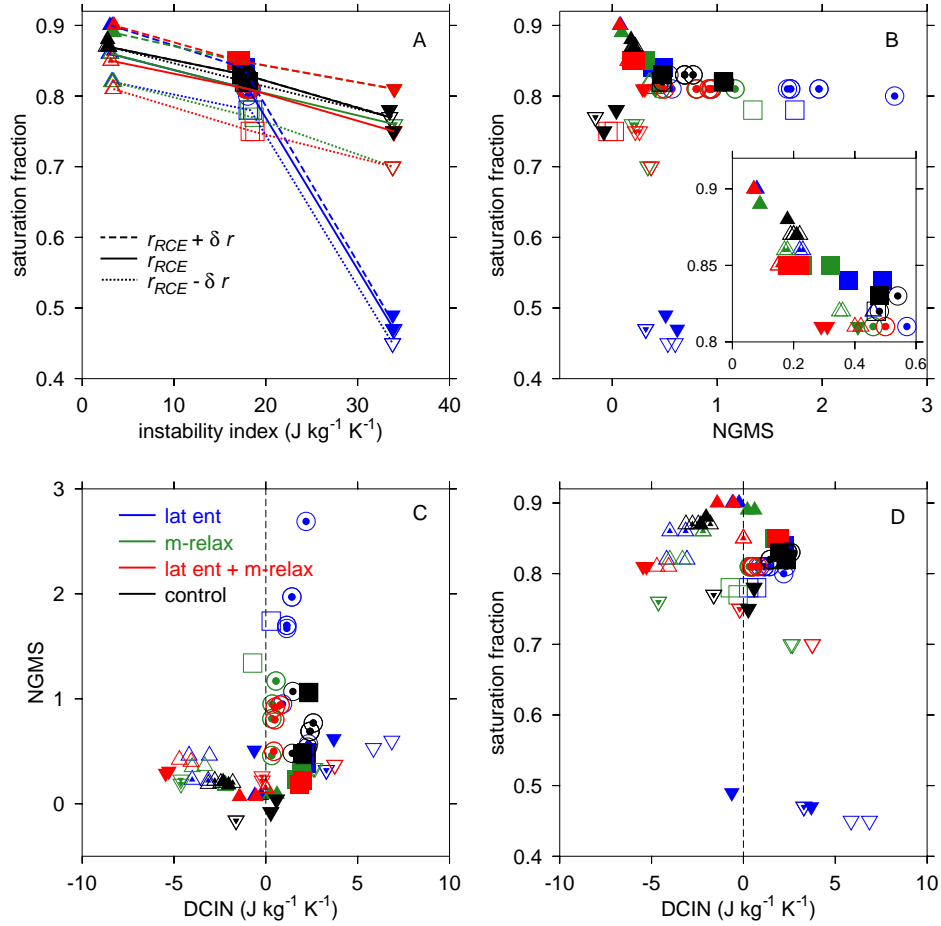


**Figure 13.** Relationships between diagnostic quantities: (a) saturation fraction vs. instability index, (b) saturation fraction vs. NGMS, (c) NGMS vs. DCIN, and (d) saturation fraction vs. DCIN. Colors indicate choice for horizontal moisture advection, while shapes indicate environmental stability and moisture according to the symbol legend defined in figure 12. Note the strong relationship between saturation fraction and instability index. As in figure 12, lines in panel (a) connect experiments with identical reference moisture profiles.

	$\lambda_{hadv} = 0$	$\lambda_{hadv} = 1$
$\lambda_m = 0$	NO	YES
$\lambda_m \neq 0$	NO	NO

**Table 2.** Table identifying which moisture treatments exhibit multiple equilibria with surface wind speed of  $7 \text{ ms}^{-1}$ . “YES” means that a dry state is maintained if initiated with a dry troposphere; “NO” means that precipitation developed in spite of an initially dry troposphere. With fixed radiation, the only moisture treatment that maintains multiple equilibria is lateral entrainment.

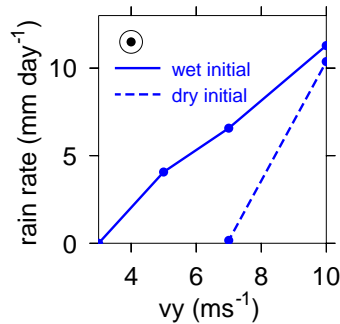


**Figure 14.** Precipitation rate as a function of surface wind speed for simulations which are initialized either with the reference moisture profile (solid line), or with a completely dry troposphere (dashed line). Moisture is laterally entrained in all experiments, and there is a range of wind speeds which exhibit multiple equilibria. The bulls eye in the upper left indicates unperturbed reference profiles (see figure 3).